TAMPERE UNIVERSITY OF TECHNOLOGY

SHAHED ALAM

HUMAN BODY EFFECTS ON RF ELECTRONICS

Master of Science Thesis

Examiners: Adj. Prof. Riku Mäkinen
Hannu Sillanpää
Examiners and Topic approved in
Computing and Electrical Engineering
Faculty Council Meeting
on 7th November, 2012.

ABSTRACT

TAMPERE UNIVERSITY OF TECHNOLOGY
Master's degree programme in electrical engineering
ALAM, SHAHED: Human Body Effects on RF Electronics
Master of Science Thesis, pages 55
June 2013
Major subject: RF Electronics
Examiners: Adjunct Professor Riku Mäkinen
Keywords: **Wearable electronics, interconnections, printed electronics, RF circuits**

Wireless sensors require radio frequency (RF) circuits to operate at close proximity to the human body. For successful design of body worn applications of electronics the study of the effect of human body on RF interconnects and simple RF circuits has been undertaken through measurements and simulations in the frequency band of 50 MHz to 9 GHz. Coplanar waveguide (CPW) transmission lines are adopted to commence the investigation. The fact that in CPW structures the ground resides in the same plane as the signal trace enables the fabrication of thin structures apt for constructing. The test structures have been fabricated using inkjet technology which being an additive and low temperature process enables the printing of transmission lines and circuit structures at which in turn enables the fabrication of test structures on thin flexible Polyethylene naphthalate (PEN) substrate. In order to discern the effect of muscle on the RF interconnections, distributed parameters, effective relative permittivity, effective loss tangent, attenuation constant and characteristic impedance are extracted using a multiline extraction process. The extraction method was also used to successfully separate the dielectric and conductor losses.

The simulations have been performed using the AWR Microwave Office commercial RF simulator. The validity of the simulations and measurements has been assessed with the agreement of the simulations with measurements. It is deduced from simulations and measurements that above 1 mm distance the losses become equal to that of free space and at 0.5 mm gap losses are close to free space as well. However, when the distance is less than 0.5 mm the losses are significant. In order to mitigate the effect of body on RF interconnects narrow gap width and centerline width should be used above 4 GHz. Bending the RF interconnects did not produce any significant change in the scattering parameters of the coplanar wave guide transmission lines, illustrating that bends do not detune the circuit performance considerably.

The effect of body on the RF circuits is analyzed using simple RF circuits of different sizes. Multiline Thru-Reflect-Line calibration has been used to extract scattering parameters of the discrete components used in the circuits. The on body simulations with AWR library components and extracted discrete component values reveal that as the length of the circuit is increased the measured components provided better convergence with measured results. The experiments performed illustrate that body has significant effect on the RF interconnects and RF circuits and the effects needs to be taken in account for proper performance of the RF circuits. The findings from the investigations are used to attain guidelines for body worn electronics design.

PREFACE

This Master's thesis is carried out in the Department of Electronics at Tampere University of Technology. The project is funded by Academy of Finland.

First and for most I would like to express my gratitude towards the Almighty ALLAH the most merciful for providing me with the opportunity to work in this educational and interesting research and also for giving me the ability to finish the task successfully. I would like to thank my supervisor and examiner Adjunct Professor Riku Mäkinen for his continual guidance and patience. I would also like thank to my supervisor Hannu Sillanpää for his assistance that he provided throughout the research work.

I would like to thank Tiiti Kellomäki for providing me with study resources that helped me to improve my writing skills which were inevitably important for my Master's Thesis. I would like to appreciate the assistance provided by the RFID research group for allowing me to use the VNA and for helping me with the instrument setup.

Lastly, I would like to acknowledge the constant support that my parents and my sister have provided me throughout the period of my Master's Thesis.

Tampere, June 2013

Shahed Alam

PUBLICATIONS

Journal publication

1. **S. Alam,** H. Sillanpaa, and R. Makinen, ”Human Body Effects on Inkjet-Printed Flexible RF Interconnections,” *Progess in Electromagnetics Research C*, Vol. 35, pp.83-94, 2013.

Conference publication

2. H. Sillanpaa, **S. Alam,** and R. Makinen, ”Printed Electronics RF Design for Body-Worn Wireless Applications,” *in Proc. IEEE Wireless Microwave Technology Conf. (WAMICON)*, Orlando, FL, 4p., Apr. 2013.

CONTENTS

TERMS AND DEFINITIONS

ABBREVIATIONS

3D	Three-dimensional
α	Attenuation constant [dB/cm]
β	Phase constant
γ	Complex propagation constant
BWE	Body Worn Electronics
C	Distributed capacitance of a transmission line [F/m]
c	Speed of Light [m/s]
CPW	Coplanar Waveguide
DC	Direct Current
EM	Electromagnetic
MoM	Method of Moments
Δ	Determinant of scattering parameter matrix
Δl	Length difference of a transmission line [m]
Δz	Length of short piece of a transmission line [m]
E	Electric Field
ECG	Electrocardiography
ε_r	Relative Permittivity
ε_{reff}	Effective Relative Permittivity
ff	Correction factor
f	Frequency [Hz]
G	Distributed conductance of a transmission line [m]
g	Gap between the signal trace and ground trace
GSG	Ground-Signal-Ground
j	Imaginary unit
L	Distributed inductance of a transmission line [H/m]
L	Length of a transmission line [m]
ω	Angular frequency [rad/s]
PEN	Polyethylene Naphthalate
PPE	Protective Personal Equipment
R	Distributed resistance of a transmission line [Ω/m]
R_{0°	Resistance in sheet resistance measurements [Ω]
R_{90°	Resistance in sheet resistance measurements [Ω]
R_a	Wave cascade matrix of error box 1

$\boldsymbol{R_b}$	Wave cascade matrix of error box 2
RF	Radio Frequency
RFID	Radio Frequency Identification
$\boldsymbol{R_S}$	Sheet resistance [Ω]
$\boldsymbol{\sigma}$	Conductivity [S/m]
S	Scattering parameters
$\boldsymbol{tan\delta}$	Loss Tangent
$\boldsymbol{tan\delta_{eff}}$	Effective loss tangent
TRL	Thru-Reflect-Line
VNA	Vector Network Analyzer
$\boldsymbol{w}$	Width of signal trace
$\boldsymbol{Z}$	Impedance parameters [Ω]
$\boldsymbol{Z_o}$	Characteristic impedance [Ω]
$\boldsymbol{Z_S}$	Series impedance [Ω]

1. INTRODUCTION

The implementation of RF circuits at close proximity to human body has grown over the years particularly in the field of wireless biosensors. Wireless biosensors are being used in wearable or implanted applications to measure heart beat, blood pressure, and other body functions [1]. In order to facilitate the growing implementation of body worn electronics a design guideline for body worn application is essential for accurate and speedy circuit design. Extensive research on the effect of human body on antenna has proven that body with its high dielectric constant and loss has a detrimental effect on antenna input impedance and efficiency [2-3]. However, not much study has been performed to understand how the body effects the interconnections and the RF circuits at varying frequencies. Nevertheless, the changes in antenna characteristics instigate the need of investigating the effect of human body on RF interconnects and RF circuits. The effect of body should reflect in the change of characteristics of transmission line that would result in impedance mismatch, alteration in electrical length, and a considerable attenuation of signal strength that would in turn result in deteriorating the performance of the RF circuit. The estimation of the loss or deterioration of circuit performance is critical in particular for biosensors placed in direct contact with the body.

The goal of the research is to attain an accurate method of simulation that would be able to estimate losses incurred due to body in RF circuits. Consequently, on the basis of the credibility of the simulation model, guidelines for RF circuit design are attained in order to facilitate body worn RF circuit design. The commercial simulation software package used for the analysis is AWR Microwave Office [6]. The Axiem Simulator integrated in AWR, facilities the construction of simulation model since, it allows diverse materials existing on top of one another in measurements to be defined in separate layers. The material characteristics of the muscle used in the simulations are obtained from [7].

One of the key features required to discern is the effect of the body on RF circuits due to its proximity. To accomplice the desired feature thin light weight flexible polyethylene naphthalate (PEN) substrate is used and coplanar waveguide (CPW) structure is adopted for the study of radio frequency (RF) interconnections and circuit design in proximity to body. The thin and flexible nature of the substrate is apt for body worn applications since, the characteristics add to the comfort of the user. The test structures are fabricated on the flexible substrate using printable electronics technology [4-5]. Inkjet electronics printing method, which is one of the members of printable electronics technology, being an additive and low temperature printing method, enables the printing of the electronics structures on the PEN substrate feasible. The desired free space and on muscle measurements are undertaken using microwave air foam and fresh

beef respectively. The measurements are performed using a vector network analyzer (VNA) that takes measurements from 50 MHz to 9 GHz connected with a probe station.

In order to attain further insight in the effect of body on RF interconnections and circuits, wide band extraction methods has been used. Hence, an improved multiline extraction method [5][-9] based on the multiline thru-reflect-line (TRL) calibration technique [10] is utilized to extract the distributed and effective characteristic parameters of the printed interconnect in free space and on muscle. Attenuation constant (α) values of the CPW transmission lines are exhibited to illustrate the variation of the losses and consequently, have been used to deduce the distance from the body that is useful for on body circuit applications. Distributed parameters, resistance per unit length (R) and conductance per unit length (G) are extracted to illustrate how the losses are distributed in the conductor and the dielectric. Effective characteristic parameters such as the permittivity (ε_{reff}), loss tangent ($tan\delta_{eff}$) and characteristic impedance (Z_o) that serve to provide useful data essential for calculating electrical length, characterizing muscle and matching impedance are extracted using the extraction method. The multiline calibration has been innovatively utilized to attain the scattering parameters for discrete components that are incorporated in the fabricated RF circuits.

The remainder of the thesis is illustrated as follows. In Section 2 few of the applications, properties of BWE is discussed and in the light of the discussion the required guidelines for BWE circuit design are illustrated. The required theoretical background is provided in Section 3. Namely CPW structure, printable electronics technology, DC measurement technique, multiline extraction method and it's utilization to obtain the distributed and effective parameters are explained in the section. Section 4 depicts of the description of fabricated test structures, measurement instruments and the description of the measurement setup. Results from the simulations and measurements and its comparisons are illustrated in Section 5. Finally, a description of the achievement of the research is realized in the conclusion section.

2. BODY WORN ELECTRONICS

The enormous popularity in mobile communication illustrates the strong liking of people on tether less voice communications. In addition to, the development in wireless communication the portability of electronic device is also one of the prominent features that attract users. The combined response for mobility and portability coupled with development in wireless technology over the past decade instigated a heave in the demand for body worn electronics (BWE). Numerous researches have been completed and evidently a lot more needs to be pursued in order to successfully provide BWE systems that would comfortably fit into people's daily life. In this section at first few of the applications of BWE are exemplified and then, desired properties of BWE electronics circuitries are discussed and based on the properties, how the characterization of some of the factors could serve to be used as guidelines for the design of BWE circuitries are discussed. Hence, this particular section is intended to illustrate the motivation of the research.

2.1. Applications

BWE have applications in diverse fields. Some of the prominent fields would be data networking, telemedicine and fashion.

One novel use of BWE system in the field of data networking, is its integration in fire-fighters clothing in order to provide them an automated personal protective equipment (PPE) system [11]. PPE apart from providing hands free communication and tracking is also able to sense the environment. The environment is sensed by means of measuring the heat and moisture in the multilayer protective fabrics that has been developed. PPE can also monitor the heart rate and is a necessary heart attack causes the most fatalities in this profession. The tracking option coupled with voice communication can help victims and in some cases fire-fighters trapped in debris to be rescued. The hands free communication also simplifies the job of fire fighters compared to the past technology where handsets needed to be used. The electronic system consist of sensors, processor and communication equipment that are implanted within the turnout coat and is transparent to the user.

Telemedicine projects requiring the application of BWE could serve to enable patients who require 24 hour observation for prolonged period such as for months and years to live at the comfort of their home. HealthService24 is one such European telemedicine projects that is seeking to provide continuous viable mobile services for health care permitting health professionals to remotely assess, diagnose and treat patients while enabling the patient to be mobile [12]. The mobility pursued is primarily intended for patients suffering in chronic diseases because of the long period of the

disease [13]. At present the remote services that are offered by HealthServices24 is done by means of wired phone and electrical lines thereby, limiting mobility. Most of the wireless medical appliances that are present in market can provide ´spot´ measurements that are only a few minute measurements that can be transmitted and stored and analyzed. Goal of projects like HeathService24 is to provide completely mobile and continuous health care service. The completion of such projects would enable reduced hospitalization, lower healthcare costs, improved quality of life and most importantly continuous healthcare service from any location of the world. Consequently, the success of such projects are essentially depended on successful design of wireless BWE devices because that would require wireless communications with wearable sensors that measure vital physiological parameters such as blood pressure, heart rate, electrocardiography (ECG), blood glucose, blood oxygen saturation, temperature etc [14-17].

Apart from the medical applications of body worn electronics there are some applications motivated not only by necessity but also by want. BWE devices can also serve as fashion accessories along with being a source of entertainment and information. In Japan for instance, mobile phones are more likely to be worn in lanyard around the neck as a colour coordinated fashion accessory [18]. Many business users on the other hand may have their Blackberries clipped in their belts in plastic holsters as hypothesized by famous futurologist Jonathan Mitchener [18]. Jackets that consist of electronic display to control the Mp3 player are already out in the market. Wireless headphone is something that is very much in use. Viable applications of BWE that futurologist think is very much possible in future are clothing that can understand human gestures, being used as speakers, microphone, camera and security identity device, key identity authentication function device integrated in clothing. The beginning of radio frequency identification (RFID) could also lead to a ubiquitous sensing network. Thus, BWE gives birth to many futuristic ideas and therefore, characterization of BWE is something that this technology demands.

2.2. Properties and Realization of BWE

In order to assimilate with human body contour and its movement BWE devices need to be light weight, flexible and unobtrusive. The flexibility of BWE devices are attained by flexible substrate. Few of the used substrates for flexible electronics are polymer film, glass, paper, ceramic and textile [19]. The selection of a certain type of substrate is application specific. Few factors that are taken into consideration in decision making would be smoothness, barrier, optical transparency, dimensional stability, thermal stability and mechanical strength/flexibility [19].

In addition to, substrate properties the other factor that is of significant importance is the choice of method by which the conducting structures would be integrated with the flexible substrate. The various method that are present are screen printing [20-22], fabrication of conducting textiles [23][24], conductive ribbons [25],

and copper meshes [26], embroidered using conductive thread [25][27] and sprayed using conductive paint [25]. Copper tapes are also used in BWE but it easily breaks and hence, it is not viable to be used for commercial purpose [26-29]. All methods have their pros and cons and hence, the choice of fabricating the conducting interconnects and conducting structures are application specific as well.

2.3. Guidelines for BWE Circuit Design

The fact that BWE circuits require to be close to human body and flexible enough to adhere to the contour of the body, the body and the bends may have some effect on the characteristics of the circuits and if so the circuits needs to be tuned for such circumstances, for the circuit to be functioning efficiently. The situation incidents certain questions the answer to which would serve as guidelines for BWE circuit design. The questions that need be answered to facilitate successful design are the following. How much proximity could be sustained for successful design of BWE circuitries? How much do the bends affect the performance? How does the substrate thickness and the dimensions of the interconnects affect the design? Hence, the research is motivated by these questions and in the pursuit of finding the answer novel method of simulation and measurements techniques would be verified and validated with one another.

3. THEORETICAL BACKGROUND

In this chapter the theoretical background of the methods and structures used in the research are explained. The transmission line and the circuit adopted for the research are coplanar waveguide (CPW) structures. A brief description of the physical properties of CPW is described. The test structures are fabricated using inkjet printing technology and hence, a short description of the method is provided. Light is shed on multiline extraction method that has been utilized to extract the electrical parameters. Transmission line parameters that would enable the change in the characteristic of the RF interconnects to be assessed are mentioned and how the parameters are obtained through multiline extraction method is derived briefly at the end of the section.

3.1. Coplanar Waveguide

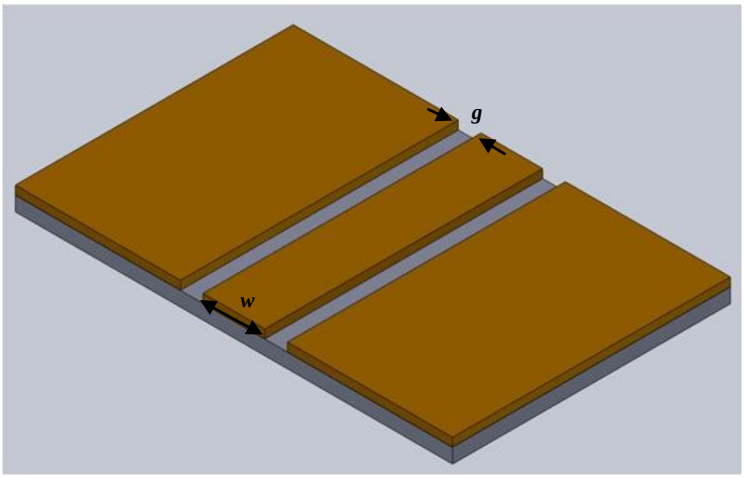

Figure 3.1. *Coplanar Waveguide Transmission Line.*

Coplanar waveguide is a transmission line, the ground traces of which lie in the same plane as the signal trace itself as shown in Figure 3.1. The fact that the ground plane and signal trace are at the same plane, shunt connected components to the ground can be made in the same side of the substrate without drilling any vias and the fabrication of interconnects becomes simple as well. At millimeter frequencies the vias do introduce parasitic inductance. The effective permittivity variation with frequency is also lower when compared to microstrip which is one of the most commonly used planar transmission lines and this enable broadband impedance matching simpler [30]. Few other desirable properties of CPW are decreased radiation losses, reduced dispersion, relatively low dependence on substrate thickness and impedance mostly depended on the gap between signal and ground trace [30]. CPW in general is cheaper, performs better and is easier to fabricate compared to mircostrip and stripline. However, there are

certain disadvantages as well such as heating effect is high, requires electromagnetic shielding in integrated applications and sometimes mechanical strength becomes an issue as well [31]. Nevertheless, the choice of CPW as test structure is dictated by necessity, because the ground being in the same plane as the signal trace enables the construction of very thin, comfortable and unobtrusive structures. Moreover, one layer printing is also easier considering the fabrication of the test structure.

The dimensions of the CPW are restricted by the ground-signal-ground (GSG) probe used for the measurements and also the highest frequency till which the measurements can be taken [32]. The parameter that restricts the dimensions of CPW is the pitch of the probe. Pitch of the probe is the distance between the signal pin and one of the ground pins and the pitch used for measurements is 800 μm. The ground probe needs to be placed at least 50 μm from the edge of the ground trace that means 750 μm can be used for *g* and the half of *w*, where *g* and *w* is labeled in Figure 3.1. For instance, when *g* is 200 μm with offset for ground 50 μm, *w* would be 1100 μm. The band till which measurements are allowed by the 800 μm is from DC to 40 GHz [32]. The maximum frequency till which measurements were performed was 9 GHz and the limit was imposed by the VNA used that allows measurements to be taken from 300 kHz to 9 GHz.

3.2. Printable Electronics

Printable electronics is a method of printing electronic structure on different substrates. Over the years as the manufacturing technologies are reaching the limits in terms of material, costs and production flexibility, the demand for printing technologies in electronics production has increased drastically [33]. Even though there are open questions regarding the durability and longevity of the circuits constructed using printing technology yet the technology has the potential to be utilized to make sturdy light weight displays, smart sensor systems and flexible and large area biomedical sensors [33]. Inkjet printing is one of the methods of printing electronics that has been adopted in the research in which the layout of the electronic circuit is handled as digital image. Inkjet printing method is completely additive; hence, the material waste is less than traditional manufacturing methods such as etching [34]. It is a drop on demand direct disposition technique of manufacturing electronics structures. Since the manufacturing method is contact less and operates at low temperature, the technology makes the fabrication on cheap flexible polymer films possible. The method of printing is very similar to the process in which an image is printed by an ink jet printer. The layout is converted to an image file and the ink ejected from the nozzle is controlled according to the image of the layout. Primary material of the ink is in form of conductor, dielectric and semiconductors and is application specific. The process of printing conductor traces is as such, first the substrate is made suitable for the deposition of the ink by surface treatment, then the ink is deposited and finally the nano

particles are united to form the conductive interconnects, by heating, the process is also known as sintering [35].

The material properties of the printable electronics structure depend on the manufacturing conditions of the manufacturing process. The conditions that affect the properties are sintering time, sintering temperature and temperature profile. Hence, variation of the conditions would vary the electrical properties of the printed conductors and dielectrics. The focus of the research being to illustrate the effect of body on printed RF interconnects and circuits, the characterization of printable electronics when held in proximity to muscle is essential for successful design of BWE. Different test structures made at different times have different properties such as different conductivity and thickness, therefore, dc conductivity measurement is described in Section 3.3 needs to be performed to incident the simulation.

3.3. Direct Current Conductivity Measurement

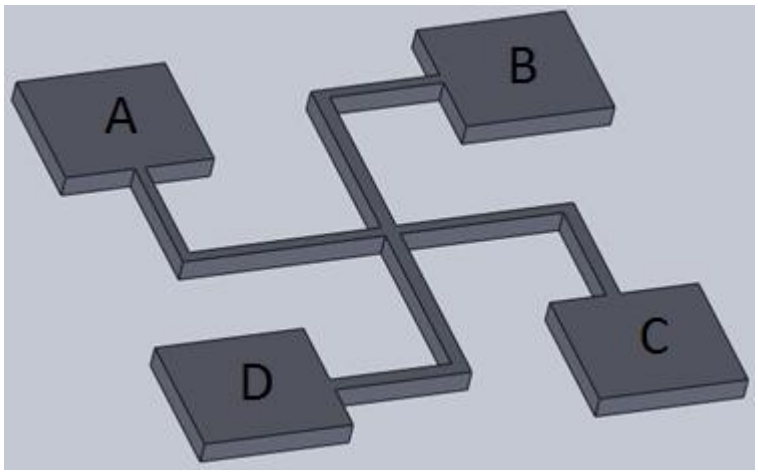

Figure 3.2. *Greek cross structure for DC measurement.*

Figure 3.2. shows the Greek cross that is used to measure the sheet resistance of the test structure [36]. It is a widely used method in the semiconductor industry [37][38]. The sheet resistance is measured by forcing current from rectangular port A to B and correspondingly measuring the voltage across D and C. Then similarly the current is forced to pass in the reverse direction and the voltage V_{DC} is measured and the resistance R_{0° is calculated as shown in equation (1).

$$R_{0^\circ} = \frac{V_{DC} - V_{CD}}{I_{AB} - I_{BA}} \tag{1}$$

The current is then required to be forced through the pads B and C and the process is repeated and R_{90° is calculated using equation (2).

$$R_{90^\circ} = \frac{V_{AB} - V_{BA}}{I_{BC} - I_{CB}} \tag{2}$$

Using equation (3) the average R of the two above mentioned resistance is calculated. The value of R is applied in equation (4) to obtain the value of sheet resistance R_S. In equation (4), *ff* represents the correlation factor that is required to compensate geometrical asymmetries of the Greek cross crossing area. *ff* is set as 1 because geometrical correction is not considered in the research.

$$R = \frac{R_{0^\circ} + R_{90^\circ}}{2} \tag{3}$$

$$R_S = ff\,\frac{\pi R}{\ln(2)} \tag{4}$$

$$\sigma = \frac{1}{R_S t} \tag{5}$$

Once the sheet resistance R_s is determined, the conductivity of the test structure can be determined if the thickness of the traces are known using equation (5). Nevertheless, it should be acknowledged that the attained value is an approximate value because the conductivity of the conductors especially at high frequency depends on surface roughness and porosity as well. Therefore, slight tuning of the conductivity value is required for simulations to comply with the measurements.

3.4. Multiline Extraction Method

Transmission line-measurement based characterization methods are suitable for characterization of both conductors and dielectrics using VNA measurements. Printable electronics can be characterized using single line-pair based characterization [39-41]. Nevertheless, the half wave resonance happening due to the difference of length of the measured lines and the high manufacturing tolerance which inkjet printed electronics structures exhibit decrease the accuracy of the method. By using the multiline extraction method the problem of half wave resonance can be avoided [40][41]. The multiline extraction methods take advantage of the redundant measurements. Typically, the redundant measurements are performed by taking measuring transmission lines of different lengths, which also increases the measurement bandwidth.

Figure 3.3. represents a transmission line section L and two error boxes R_a and R_b. The error boxes models the transition from the probe-head to the transmission line and other possible discontinuities and pad parasitics at the line ends. The characterization process begins with the first tier calibration moves the known reference

Figure 3.3. *Transmission line consisting of two error boxes R_a, R_b and a central length of L.*

impedance at the tips of the probe. The multiline material characterization is divided in two steps: first phase is to solve the propagation constant of the lines and error boxes at the ends of the lines through the TRL calibration [43]. The multiline TRL calibration weights the measured transmission lines and selects the optimal propagation constant and error boxes at each frequency points. The second phase is to fit an equivalent circuit to the error box network parameters such that the characteristic impedance of the transmission line is solved from it. For printed transmission line multiline extraction method has been found to be most apt for characterization [44].

3.5. Distributed Parameters

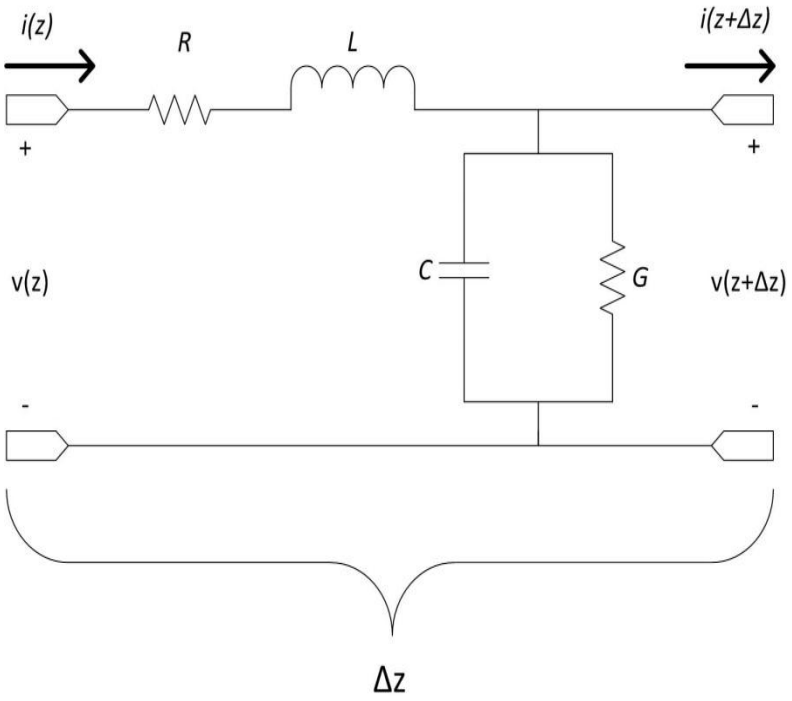

Figure 3.4. *Lumped circuit equivalent circuit of transmission line.*

Transmission lines at microwave frequencies are a fraction or several wavelengths long hence, the voltage and current along the length of the transmission line may vary in phase and magnitude. Therefore, in order to characterize transmission line at high

frequencies transmission lines are represented as distributed parameter networks. Figure 3.4. represents a Δz section of transmission line that is the length in which the distributed parameters *R*, *L*, *G* and *C* are constant [45].The series inductance *L* is the total self-inductance between the conductors and the shunt capacitance *C* represents the capacitance due to the proximity of the conductors. The series resistance *R* represents the finite conductivity of the conductors and the shunt conductance *G* is due to the dielectric loss between the conductors. Applying Kirchhoff's law in Figure 3.4. and adopting some assumptions, derivatives and substitution the expressions obtain for propagation constant and characteristic impedance are provided in equations (6) and (7).

$$\gamma = \alpha + j\beta = \sqrt{(R + j\omega L)(G + j\omega C)} \tag{6}$$

$$Z_o = \sqrt{\frac{(R + j\omega L)}{(G + j\omega C)}} \tag{7}$$

Squaring and substituting equations (6) and (7) the deduced expressions for distributed parameters are provided in equations (8) to (11).

$$L = lm\left(\frac{\gamma Z_o}{\omega}\right) \tag{8}$$

$$C = lm\left(\frac{\gamma}{Z_o \omega}\right) \tag{9}$$

$$R = Re(\gamma Z_o) \tag{10}$$

$$G = Re\left(\frac{\gamma}{Z_o}\right) \tag{11}$$

The distributed parameters can then be used to further extract useful parameters which are essential to perform electromagnetic simulations (EM) and design radio frequency (RF) circuits. Equations (12) is used to calculate the permittivity where *c* is the speed of light in vacuum, β is the imaginary part of the propagation constant known as phase constant as well and ω is the angular frequency. Real part of the permittivity is calculated using equation (13) *C* is capacitance per unit length and Z_C is the characteristic impedance. Equation (14) enables the loss tangent value to be calculated [44].

$$\varepsilon_r = \left(\frac{c\beta}{\omega}\right) \tag{12}$$

$$\varepsilon_r = Re(cCZ_o) \tag{13}$$

$$tan\delta = \frac{G}{C\omega} \tag{14}$$

To summarize, the distributed parameters of the transmission line are obtained from the propagation constant and characteristic impedance values extracted from the calibration. The obtained parameter values can then be used to obtain the other effective parameters of the CPW transmission line. This method is well suited for wide band characterization of electrical material properties in printable electronics.

4. SIMULATION MODEL

The simulation model requires being such that the varied materials that are included in an on body simulation can be modeled. The materials being air, inkjet printed conductor traces, substrate and the body. Moreover, the characterization of the materials over the entire frequency range is of eminent significance so that the results obtained are credible. Therefore, careful analysis requires to be made in selecting the simulator and characterizing the material parameters. In this section the process of defining the material parameters and the integration of the materials in simulation model would be illustrated elaborately.

4.1. Test Structure

In order to make the modeled CPW transmission lines similar to the actual test structure the sheet resistance and dimensions are required to be known prior to simulations. Moreover, as already been stated in Section 3.2. the characteristics of inkjet printed structures vary considerably from one another because there are many conditions influencing the characteristics. In Figure 4.1. the test structure that consists of varying length of coplanar waveguide (CPW) transmission lines is displayed. The single layer CPW is selected due to its suitability for the printing process and tot realize the thin lightweight required for BWE. The CPW traces are made of silver nano particle conductor and the traces are printed on 50 μm PEN substrate. The test structure consist of CPW of length 31mm, 25 mm, 19 mm, 11 mm, 9 mm, 5 mm , 1 mm and Open. The Greek crosses that are visible in the test set in Figure 4.1. are used

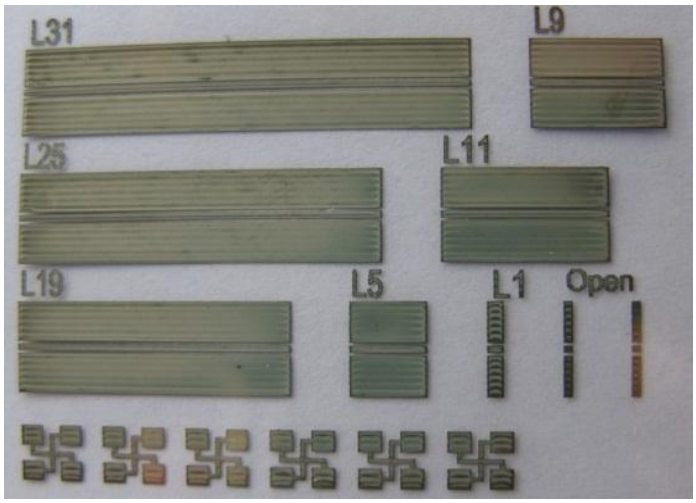

Figure 4.1. *Inkjet printed coplanar transmission line on PEN substrate*

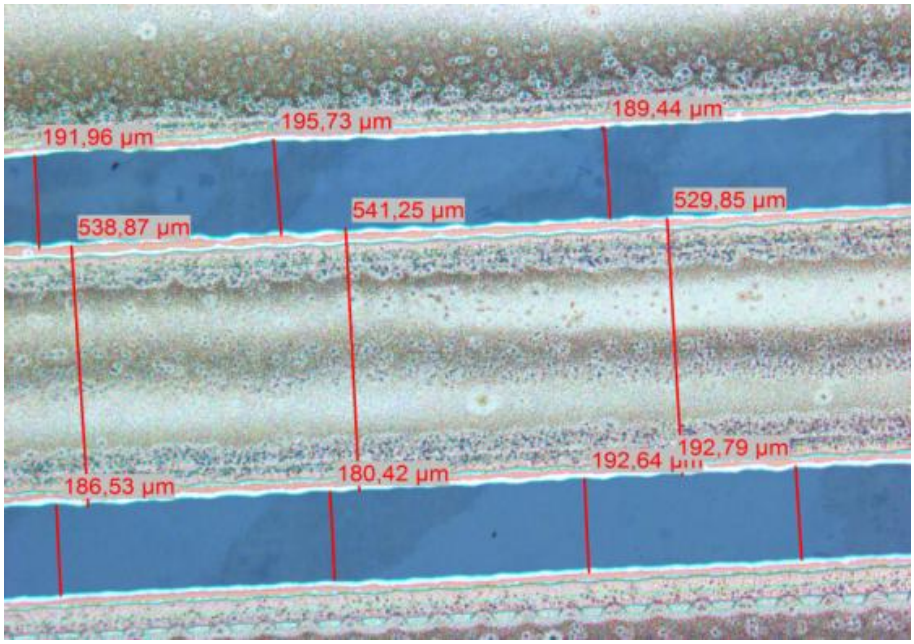

Figure 4.2. *Microscopic view of inkjet printed coplanar waveguide transmission lines*

to measure the sheet resistance *Rs*. The average value of the measured *Rs* is 105 mΩ. Figure 4.2. shows the microscopic top view of CPW with dimensions of the conductor gap and centre conductor width at different positions of the CPW. It can be observed from the figure that centre line on an average is 535 µm and the gap width between the centre line and ground is 190 µm. The average value of the CPW gap and centre conductor was found to be 190 µm and 520 µm, respectively, and these values were also adopted in simulations.

4.2. Choice of Solver

AWR simulation software has been used to model the on body CPW and filter. The choice of software has been considered because of the integrated three dimension (3 D) method of moment (MoM) electromagnetic (EM) simulator titled as Axiem simulator [6]. Axiem simulator allows different material types to be assigned in layers on top of each other and this particular feather is apt for defining the different material types required for on body simulations. In addition, Axiem consists of direct default internal solver that accurately simulates the losses such that the losses per unit length are irrespective of length. Direct default solver assumes least approximation compared to other offered internal solvers and the direct default solver chooses between low and high direct solver that alters and adapts the mesh relative to the frequency of simulation. The required accuracy comes at the cost of prolonged period of simulation. Nevertheless, to perform meaningful simulations of inkjet printed circuits on body the direct default solver of Axiem simulator needs to be used because all the internal solvers have been tested only direct default solver was able to produce meaningful results. Therefore, the finding that needs to be restated is that, if AWR is adopted for

estimating the losses for on body simulations Axiem simulator and its internal direct default Solver is the only means to attain desirable results.

4.3. Modelling and Characterization of CPW on Body

The simulation models consist of 4 layers. The first layer consists of the three conductors of equal length. Two of the conductors that are of equal width (3 mm), forms the ground traces and between the grounds the signal trace is placed, thus forming the CPW. Figure 4.1. shows the printed CPW lines and Greek crosses. The Greek crosses have been used to perform DC measurements in order to measure the sheet resistance R_S. Using R_S and assuming a suitable thickness of the conductor the conductivity of the test structure can be calculated. The description of the DC measurement process and calculation of conductivity has been illustrated in Section 3.3. The value of R_s used in the simulations is 105 mΩ and the assumed value of thickness is 1 μm and the obtained conductivity is 9.5e6 S/m. Simulations prove that the results are depended on the product of the thickness and conductivity therefore, assuming the thickness does not add any inaccuracy as long as the R_S is kept constant. The dimensions of CPW adopted in the simulations as mentioned in the Section 4.2. are centre line width 520 μm, gap of 190 μm and the ground width 3 mm.

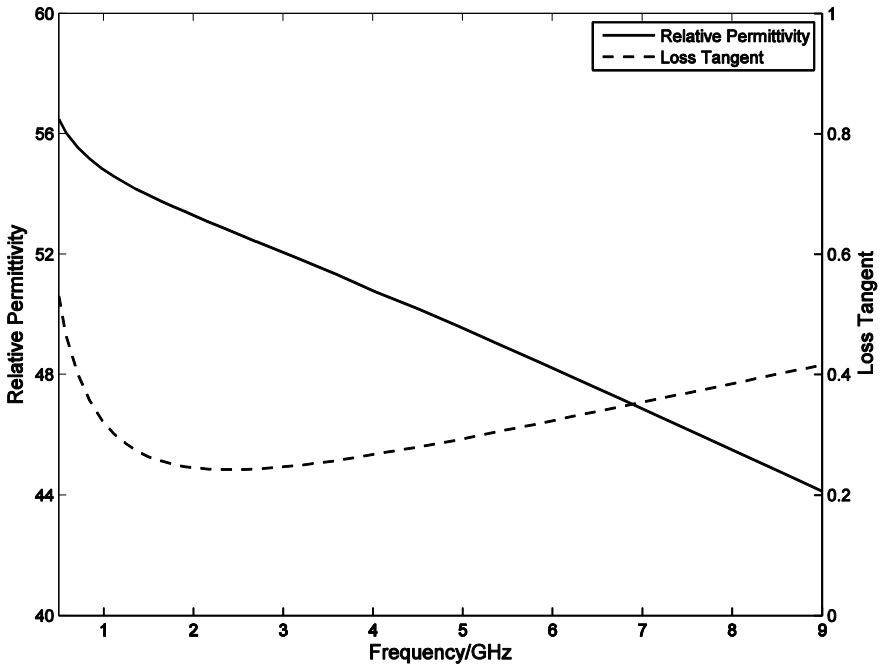

Figure 4.3. *Electrical material properties for muscle tissue [7].*

After the conductor parameters are defined, in order to emulate the printed traces on PEN substrate, the substrate parameters are defined. Three parameters that describe the characteristic of the substrate are tanδ, ε_r and t thickness of the substrate. Typical values of PEN substrate parameters are assigned, the value of tan δ is set to

0.01, ε_r is assigned as 3.35 and lastly t is defined as 50 μm [19]. The third layer represents the air gap and is the only variable and optional layer in the simulation model. By varying the thickness of the air gap the proximity to body is altered. In case of on body measurement, the third layer is excluded and consequently, the fourth layer that is the body becomes the third. The characterization of fourth layer is similar to that of second layer that is by defining *tan* δ and ε_r. The values have been adopted from a website providing dielectric properties of different body tissues from frequency range 10 Hz to 100 GHz [7]. The website is certified by national council of applied science of Italy. The parameters values are interpolated in graphs in Fig.4.2. In the simulations the values of the parameters are placed inform of frequency depended equations.

To summarize the order of assigning the four layer of the simulation model is as follows, conductor traces, substrate, air gap and body. In the first layer for the conductors' conductivity and thickness are assigned and last three dielectric layers loss tangent, permittivity and thickness of the corresponding layers are defined accordingly.

4.4. Demonstration of the Constructed Model

Low-pass filters were designed to investigate the effect of human body on discrete RF circuits. 5th order low pass filters is used. The values of the components are calculated using coefficients provided in the table [45]. For attaining the S-parameter at the terminals of CPW, EM simulation was enough but in case of filters where discrete components are involved the interconnections and the components needs to be modeled together and simulated. Unfortunately, the EM simulations do not allow the addition of discrete components, so EM structures are required to be added in the schematic of the filter structures. Extract is a simulation control block available in AWR that enables to associate the discrete components introduced in the schematic with the interconnection via a physical simulation of the layout of the individual components.

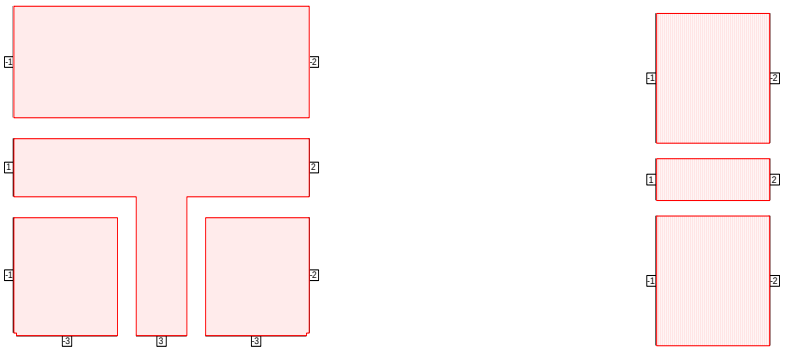

(a) (b)

Figure 4.4. *(a) EM layout of T – shaped CPW interconnection. (b) EM layout of straight CPW interconnection.*

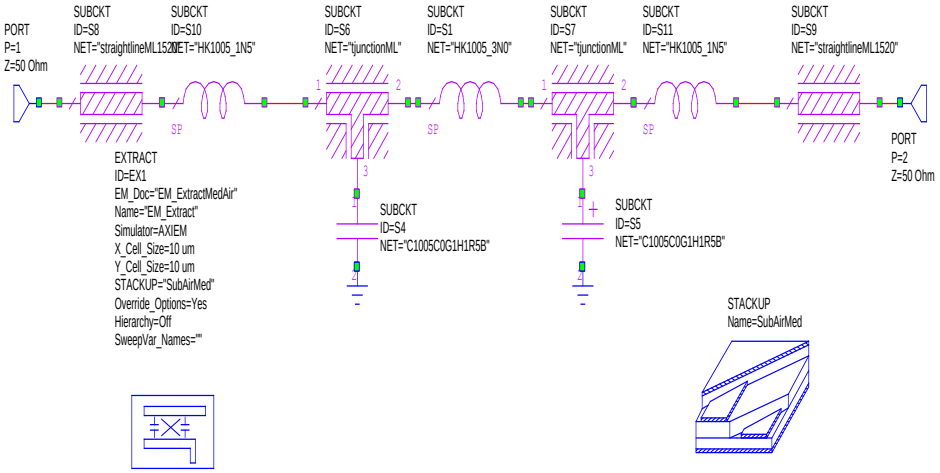

Figure 4.5. *Schematic of 5th order low pass filter, with EXTRACT block to connect the schematic with EM interconnections and STACKUP block to define the substrate parameters.*

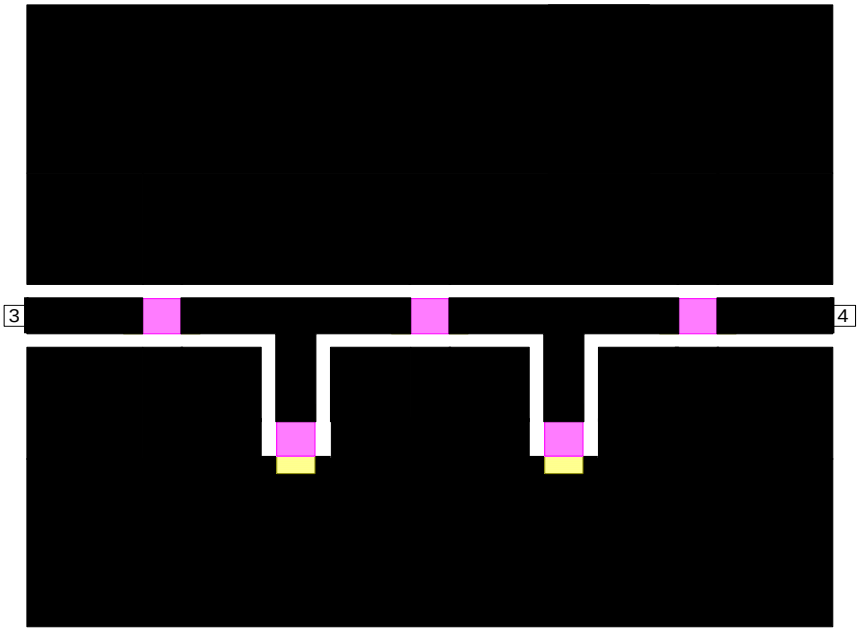

Figure 4.6. *EM Layout of the low pass filter attained from extraction*

In Figure 4.5. the circuit components are defined as general sub circuit elements. For the capacitors and inductors the corresponding S-parameter files are assigned to it. For the interconnections the EM structure of the interconnection shown in Figure 4.4. (a.) and Figure 4.4. (b.) is attached to the sub circuit elements. Symbols are fixed to each of the sub circuit components accordingly for identification of the structures. Once the circuit components are defined, the EXTRACT and STACKUP

box are placed in the schematic. In the Extract block the simulator name, cell size and the name of the EM layout that is extracted from the extraction process are defined. In the STACK block the substrate parameters which in this case is a multi-layer non-homogenous structure is defined. Figure 4.6. shows the EM layout of the entire filter that is obtained through the extract block. Therefore, the method enables the EM simulation to perform in the entire structure and thereby, also enabling the use of Direct Default solver to be used for simulating the interconnecting inkjet printed structures.

4.5. Validation of Simulations

The target of research is to construct a simulation model that would be able to estimate losses incurred when an RF circuit is placed close to the body. For simulation models to be accepted as credible the results obtained from the simulations needs to match with the measurement results. The first target is to attain agreement between the CPW free space simulations and measurements results. Once the simulations and measurement results for free space agrees, the parameter values of the substrate and conductors obtained from the simulations could be used for body simulations. If the on body simulations and measurements agree with one another than it can be concluded that the simulations are accurately estimating the losses. That is the simulations and measurements needs to agree at both ends namely, in free space and on muscle. After the simulation model is validated the research can be extended to investigate the effect of varying air gap, effect of varying g and w of CPW, effect of varying substrate thickness and finally the effect of muscle on RF circuits. The research is particularly meaningful because the success of the simulation model would enable the research to be extended to model complicated circuits such as bio sensors that needs to operate at close proximity to human body.

5. MEASUREMENT SETUP

In this section the two platforms in which the measurements are performed are introduced. The measurement setup includes the instruments involved and the test structure that is fabricated would be depicted. In addition, the precautions the measurement requires would be elaborated as well. The measurement setup can be divided in two parts. The first part consists of the devices used and calibration of equipment. The second part includes the materials used in the measurement and the process in which the measurements are performed.

5.1. Measurement Devices and Calibration Process

The instruments that have been used to undertake the measurements are E8358A PNA 300 kHz - 9 GHz and microwave probe station. It has been observed that the measurement of the interconnections in the thin flexible substrate is very sensitive to calibration. The measurements were first attempted with SOLT calibration [48] but the goal of separating the dielectric and the conductor loss could not be achieved. Hence, to deal with the situation Line-Reflect-Match (LRM) calibration has been adopted [48]. The better calibration is because in LRM match is the only standard which needs to be defined, thus error induced due to improper input parameter characterization of open or short standards are avoided [48]. LRM calibration was used to calibrate the Agilent E8358A PNA using the impedance standard substrate via Cascades's Wincal software. The validity of the measurements was justified by the repeatability of the measurements and in each measurement it was ensured that the S11 and S22 are identical in order to ensure that the port impedance and contact is similar. This particular fact makes the measurements in muscle difficult to execute because the platform is soft.

5.2. Measurement Procedure and Test Structures

The objective of the measurements is to obtain the S-parameter of the interconnections and filters in free space and muscles. Hence, the same CPW lines and filters are measured in two different platforms. In order to emulate free space measurements the platform used is microwave air foam that has a permittivity close to 1 and to imitate the muscle, fresh beef has been used as the base. Figure 5.1. shows the measurement setup for the muscle measurements. The muscle is covered with a thin plastic in order to protect the microwave probe station and the transmission line printed in the PEN substrate. The 800 μm probe pair is placed down in 31 mm CPW transmission line. It has been observed in the measurement that the freshness of the beef affected the loss of the measurements. Therefore, to attain acquired results the beef should not be dried. For

free space measurements the same measurements are performed but the beef is replaced with microwave air foam.

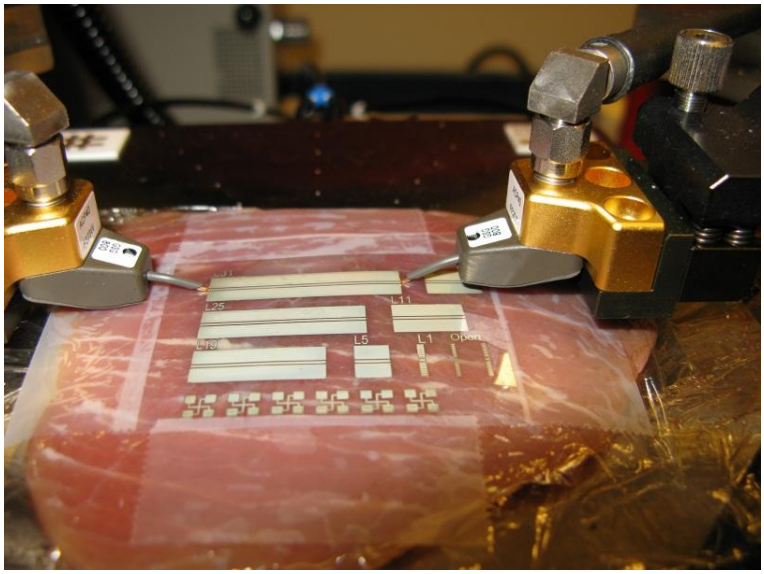

Figure 5.1. *CPW transmission line measurements in microwave probe stations on muscle.*

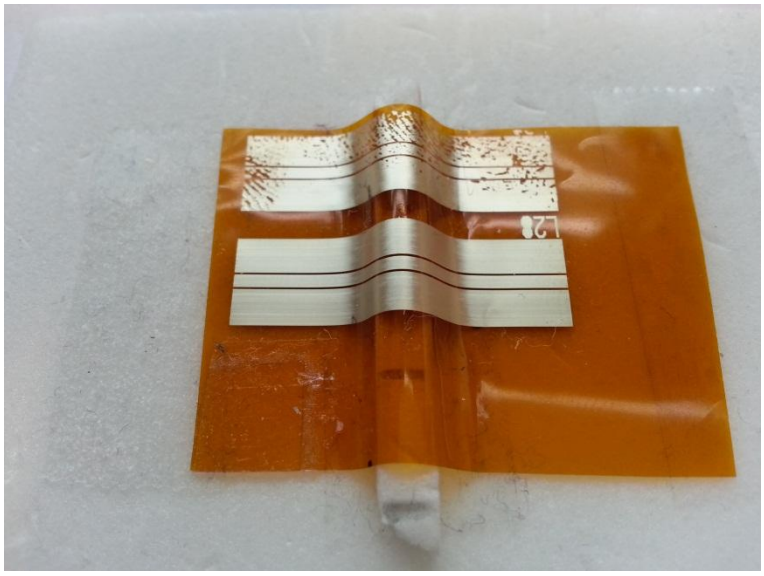

Figure 5.2. *CPW transmission line on microwave air foam, 1.2 mm diameter bend produced by a piece of microwave air foam.*

Figure 5.2. shows a bent CPW in order to investigate the effect of bending on RF interconnects. It is necessary that the bend is incumbent with air in order to mimic the bends that normally originates in BWE circuitries and hence, 1.2 mm diameter bend has been made by a piece of microwave air foam. The measurements can only be performed with lines with a length in excess of 19 mm if the diameter of the bends is

more than 1.2 mm. Since, the probe heads are very fragile it is necessary both the ends of the measured CPW is attached with the microwave air foam or else the 0.5 mm sliding of the probe in order to attain proper contact could very easily deform or damage the probe heads. Bend of diameter 4 mm has also been measured in order to further verify the effect.

Figure 5.3. *Measurement of components in PEN substrate.*

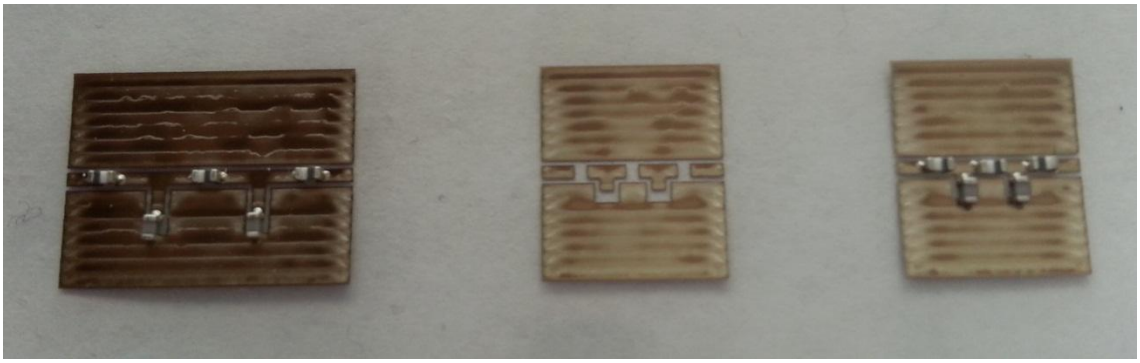

Figure 5.4. *Filter CPW structure on PEN substrate.*

Figure 5.3. shows the measurement setup of the distributed components on muscles. Three filter structures are displayed in Figure 5.4. The figure consists of filters of two dimensions. Filters located in the centre and in the right of the substrate are of the same dimensions and the horizontal length of the filters is 7.2 mm. The longer filter located in the left has a horizontal length of is 11.2 mm. The components of the filters are placed by blowing hot air in the pasting fluid. The centre line is 520 μm and the gap is 190 μm. Figure 5.3. shows the measurement setup of the 0402 inductors and capacitors mounted on PEN substrate placed over the muscle. On the right of the figure an image of the components placed on the PEN substrate also displayed.

6. RESULTS

In this section the results from simulations and measurements are compared and the information attained from them is elaborated. One of the objectives of the research was to validate whether the simulations matches with the measurements and also to find whether commercial RF simulator can be used to model the body effects. It has already been mentioned in the previous section that the dielectric loss and loss tangent of muscle is frequency dependent and the hypothesis of the research was also such that in measurements the muscle would behave in similar manner. Hence, this being the result section the credibility of the hypothesis would be assessed. Building on the validity of the simulation and measurement results of the RF interconnects the research would be extended to observe the effect of human body for other orientation of RF interconnects and then finally to RF circuits. The section is broadly divided in two parts, the first illustrate the results of the RF interconnection and the other would elaborate on the simulations and measurements of low pass filters.

6.1. Analysis of Air Gap on RF Interconnects

Multiline extraction method is used to obtain from the S-parameters obtained from simulations and measurements to attain the required parameters that define the characteristics of CPW transmission lines. Single line-pair based characterization methods are used for plotting the characterization parameters for simulated CPW. However, because of the relatively large manufacturing tolerances associated with inkjet printed transmission lines and the half-wave resonances multiline extraction method, is used for the printed lines instead of single line pair method.

6.1.1. Attenuation Constant

The attenuation constant is the sum of dielectric loss, conductor loss and radiation loss. The radiation loss is significantly lower than the dielectric loss and the conductor loss hence, the attenuation constant can be considered as the sum of dielectric and conductor losses. In other words, attenuation constant depicts the attenuation of a signal, that the signal experiences as the signal propagates through transmission medium. In Figure 6.1. the simulated and measured attenuation constant curves are exhibited in the frequency range of 50 MHz to 9 GHz. It can be observed from the figure that the free space simulation and the measurement on low-loss microwave foam curves located in the bottom of the overlap with one another. The overlapping depicts that simulation of on air measurements agrees with the measurements. A third curve that also overlaps with the free space simulation curve is the simulated curve for 1 mm air gap. This reveals that if the interconnects are 1 mm away from the body the effect of body is negligible. In order to further ensure the credibility of the simulations, on muscle

measurement needs be compared to the in contact simulation. The Figure 6.1. reveals that the on muscle measurement curve lies 0.7 dB lower than the curve of the in contact simulation. However, the difference could be explained with the 10 µm air gap simulated curve that lies at close proximity to the on muscle measurement curve.

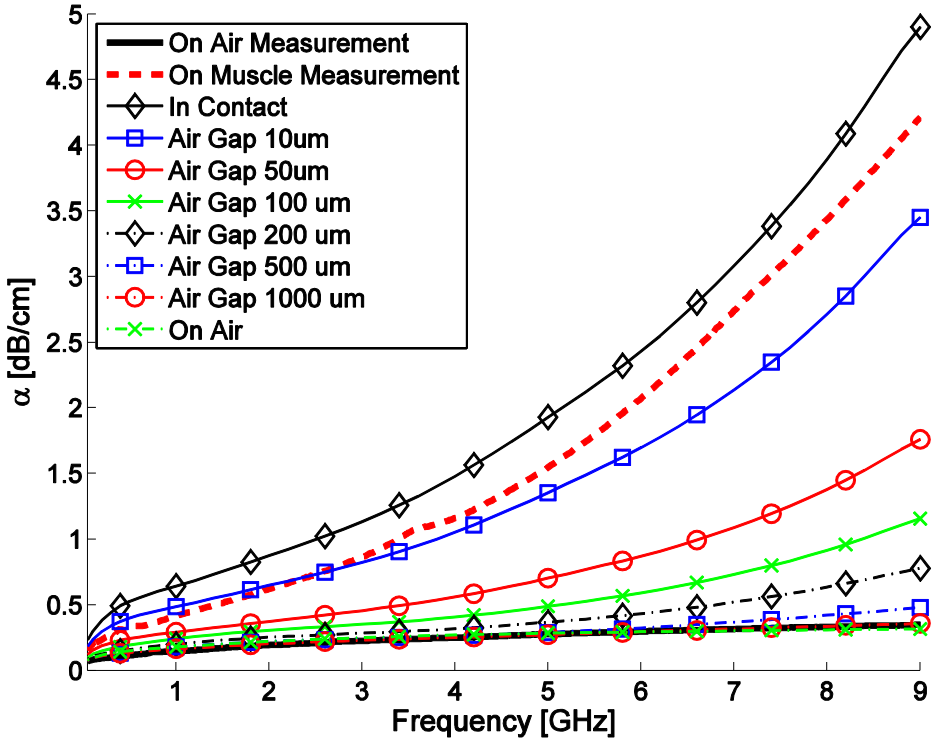

Figure 6.1. *Extracted Attenuation Constant values in the frequency band of 50 MHz - 9 GHz from simulations and measurements.*

The fact that there is a thin plastic covering the beef and a possible film of air which could be in the order of 5 µm to 10 µm that inevitably cannot be removed is the practical reason for the 0.7 dB difference. Nevertheless, the shape of the curves also validates the reliability of the simulations as well. The steepness of the curves beyond 4 GHz is increasing as the proximity to the body is decreased and the steepness complies with the two extreme that is the free space and on muscle measurements. As the air gap is increased from 10 µm to 50 µm, the value of α (dB/cm) at 9 GHz decreases drastically from 3.5 dB/cm to 1.8 dB/cm. The change at 9 GHz is considered because the divergence is most prominent at the highest frequency point which is as expected since the fluctuation of the electric field is the maximum at the highest frequency resulting greater dielectric loss and also the skin depth decreases that in turn adds to conductor loss. As the air gap is further increased beyond 50 µm, the α (dB/cm) slope and the gap between the curves changes more gradually. When the RF interconnects is placed 0.5 mm away from the body the attenuation constant lies very close to that of the free space measurements and the curve is located below the 0.5 dB/cm throughout the observed frequency band. Hence, the effect of body on RF interconnects when placed at

0.5 mm away from the body the effect of body may not be that significant. Table 6.1 provides the frequencies below which the attenuation constant is less than 0.5 dB/cm, at different distance proximity to the muscle. The table also illustrates that for BWE applications the gap less than 0.5 mm can also be acceptable if the frequency is less than 9 GHz.

Table 6.1. *Frequency below which the attenuation constant is below 0.5 dB/cm.*

Proximity / µm	In contact	10	50	100	200	500
Frequency / GHz (α < 0.5 dB/cm)	0.3	1	3.2	5	7.2	9

6.1.2. Resistance Per Unit Length (Conductor Loss)

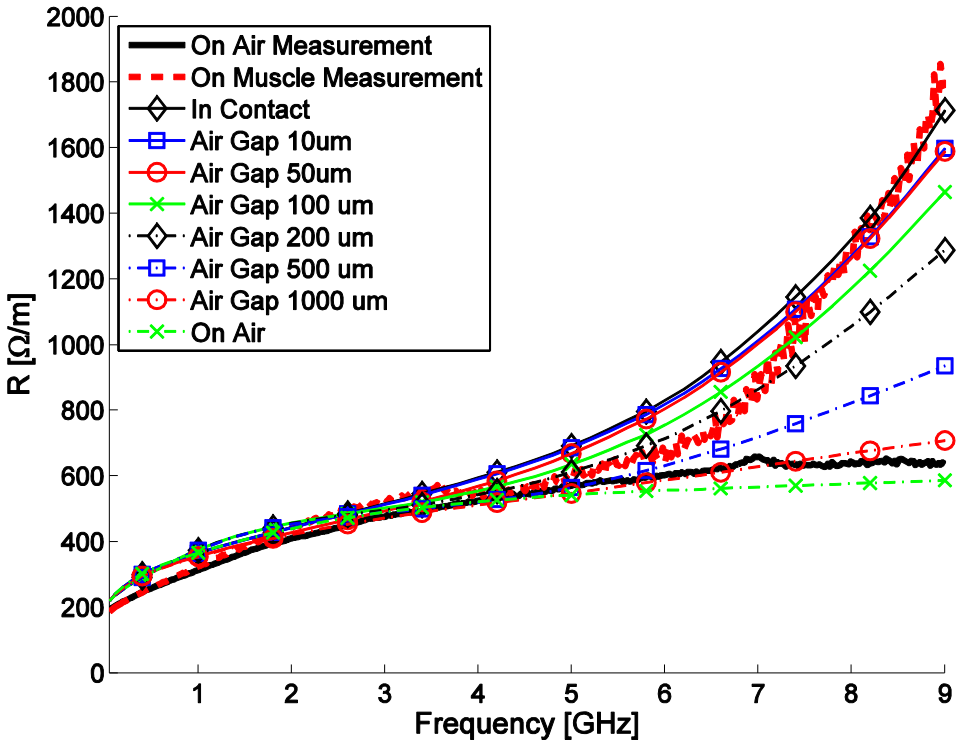

Figure 6.2. *Extracted Resistance per unit length values in the frequency band of 50 MHz - 9 GHz from simulations and measurements.*

Figure 6.2. shows how the resistance of the measured CPW transmission lines varies as the proximity to body of the interconnects and the frequency are varied. *R* represents the finite conductivity of the transmission line and because of skin depth as the frequency increases the resistance should also increase. The curves in Figure 6.2. is arranged in similar order as in Figure 6.1. In air and on the muscle curves envelopes the

simulation curves for different air gaps. The air gap that were considered useful to illustrate the gradually change of characteristics properties are 10 μm, 50 μm, 100 μm, 200 μm, 500 μm and 1000 μm which is same as in Figure 6.1. It can be seen from Figure 6.2. that all the curves have similar *R* (Ω/m) below 5 GHz illustrating that the conductor loss is independent of air gap below 5 GHz. This phenomenon is expected because the dimensions and the thickness of the conductor traces on which the loss power depends, remains the same in all simulations and measurements. Nevertheless, a drastic increase in the resistance values is observed as the frequency increases, indicating that the interconnects becomes sensitive to proximity of muscle when the frequency is above 5 GHz. The fact that the phenomenon is present in simulations and measurements verifies the occurrence is real. Simulations have been performed in which the conductors are made to be perfect conductors (*R*=0) and the same phenomenon is observed over muscle. Hence, a theory can be deduced that the muscle beyond 5 GHz the muscle starts to act as a lossy ground plane, which is causing the exponential shaped rise in the resistance value. Thereby, the losses that are reflected in Figure 6.2. are not totally due to skin depth but primarily due the muscle underneath the substrate or multiline extraction methods fails to separate the dielectric and conductor losses.

Table 6.2. *Resistance per unit values at different frequency points on three different platforms on Air, in 0.5 mm Air Gap and on Muscle.*

Frequency (GHz)	Resistance per unit length (Ω/m)		
	On Air Measurement	Simulation with 0.5 mm Air Gap	On Muscle Measurement
5	573	564	599
6	603	631	641
7	658	719	875
8	641	821	1278
9	636	935	1801

Table 6.2. illustrate that the change in resistance value when on air is 63 Ω/m as the frequency increases from 5 GHz to 9 GHz. The change in the frequency band is about 371 Ω/m when the air gap is 0.5 mm. In case of in contact measurements, the change in resistance increases to approximately 1202 Ω/m. Considering, on air measurement the rise is solely due to skin effect attenuation or in order words conductor loss. Hence, the increase of (1202 Ω/m-63 Ω/m) 1139 Ω/m in the muscle measurements as the frequency is increased from 5 GHz to 9 GHz is due to the muscle acting as a lossy ground plane. Thus, what appears to be rise in conductor loss is in reality loss added by the muscle acting as lossy ground plane. As the air gap is increased from 0.5 mm to 1 mm the resistance value converges with the on air simulation and measurement results.

6.1.3. Effective Loss Tangent (Dielectric Loss)

In EM simulations one of the essential parameters to characterize the substrate material is loss tangent. Hence, to characterize muscle in BWE application simulations the effective loss tangent value at the frequency of design is critical for RF circuit designers. Figure 6.3. shows the variation of the loss tangent in the frequency band of 5 GHz to 9 GHz. The results are provided in similar order as Figure 6.1. and Figure 6.2. The in air simulation and measurement curves do converge fittingly with each other throughout the frequency band. The muscle measurement curve complies with the 10 µm air gap curve till 2 GHz. The curve diverges beyond 2 GHz and the slope of the measurement curve increases. At 5 GHz the on muscle measurement curve crosses over the in contact simulation curve. When measurements are taken on muscle it is practically impossible to ensure that the probes have exactly identical contacts at both ends of the transmission lines and since more than one transmission lines needs to measured some

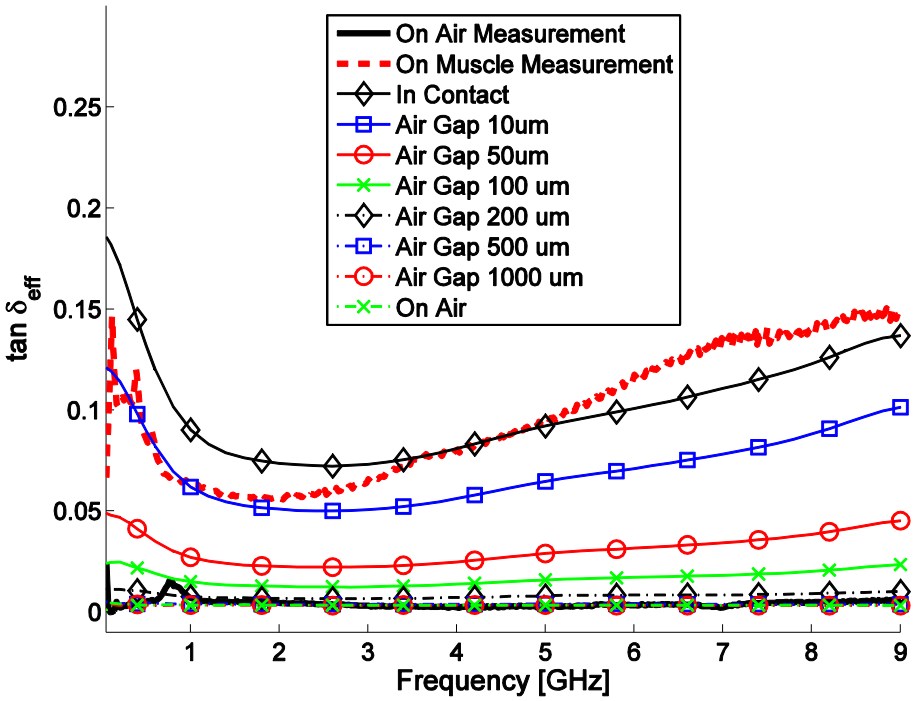

Figure 6.3. *Extracted Effective Loss Tangent values in the frequency band of 50 MHz - 9 GHz from simulations and measurements.*

aberration is inevitable. Nevertheless, the fact that the curve is wavering near the in contact simulation curve signifies the credibility of the measurements and simulations. The dielectric loss incidents from two sources, the first would be because of dielectric damping and the second being the conductivity. The imaginary part of permittivity and the conductivity contained in the loss tangent expression takes account of both of the

phenomenon resulting dielectric loss. However, at microwave frequencies considering the permittivity of PEN substrate the dielectric damping does not significantly contribute to the dielectric loss, it is the conductivity present in the dielectric medium that adds to loss significantly.

Table 6.3. *Tabulated values of Effective Loss Tangent for Interconnects in contact with body and in air.*

Frequency/GHz	Effective Loss Tangent ($tan\ \delta_{eff}$)		
	On Muscle Measurements	On Muscle Simulation	On Air Simulation
1	0.0621	0.0915	0.0148
2	0.0561	0.0735	0.0126
3	0.0658	0.0715	0.0125
4	0.0781	0.0808	0.0137
5	0.0948	0.0921	0.0159
6	0.1174	0.1007	0.0171
7	0.1335	0.1106	0.0182
8	0.1406	0.1229	0.0201
9	0.1469	0.1368	0.0234

Table 6.3. shows that there are some differences in the effective loss tangent values between simulations and measurements at low frequencies but values are at the same order and at higher frequencies the values are considerably closer. The values on an average vary from 0.09 to 0.13 as the frequency is increased from 1 GHz to 9 GHz. The in air measurements are provided to illustrate the amount of change that incurs when the muscle is brought in contact with the CPW. The effective loss tangent value in air varies 0.014 to 0.023 as the frequency is increased from 1 GHz to 9 GHz.

6.1.4. Characteristic impedance

The characteristic impedance of a transmission line is the ratio of the voltage and current independent of position for an infinitely long transmission line. The concept of infinitely long transmission is achieved practically by matching the load with the input impedance of the transmission line. In matched conditions there are no reflections hence, the impedance becomes independent of position. Figure 6.4. shows the real part of characteristics impedance of the transmission line obtained from simulations placed at different distances from the muscle. The data in Figure 6.4. is particularly important for impedance matching. The figure shows that in air measurements and simulations lies in close proximity to one another and the on muscle measurement curve and for 10 μm air gap curve converges with one another as well. At 9 GHz the in contact impedance value is 53 Ω in measurements and 41 Ω in simulations. As the body is brought closer to the muscle, the impedance value due to dielectric loading changes

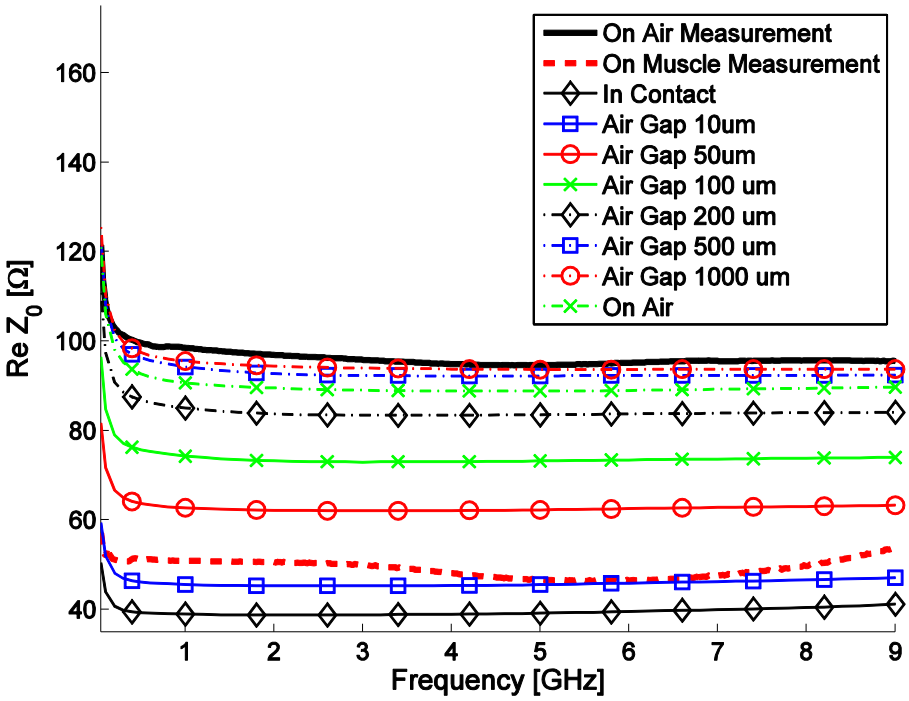

Figure 6.4. *Extracted Real part of Characteristic Impedance values in the frequency band of 50 MHz - 9 GHz from simulations and measurements.*

from 95 Ω in air to 50 Ω on muscle. Table 6.4. lists few of the values that would be valuable for consideration for attaining adequate matching for BWE circuit design. The tabulated value of impedance is an average value and is obtained from three different frequency points of the same curve. The table values illuminate that with 0.5 mm air gap the impedance becomes very close to that of free space.

Table 6.4. *Real part of Characteristic Impedance value for RF interconnects placed at different proximity to the muscle and in free space.*

Position	Average value of real part of characteristic impedance/Ω
On Muscle (Measurement)	50
Air Gap 100 µm	84
Air Gap 500 µm	90
In Air (Measurement)	95

6.1.5. Effective Permittivity

Figure 6.5. display the effective permittivity values on the frequency band of 50MHz - 9 GHz. The coplanar transmission line being an open structure the electric field lines extends both in air and substrate. The field extends below in air foam and muscle as well. Therefore, effective permittivity needs to be known in order to determine the phase shift or electrical length of the interconnects. Figure 6.5. serves to provide the

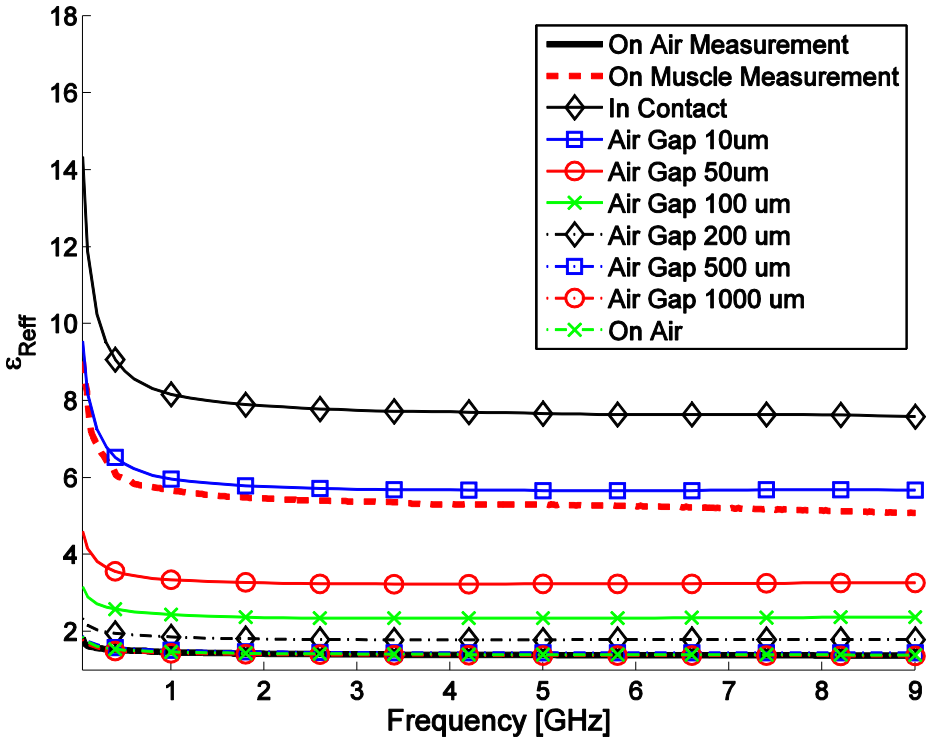

Figure 6.5. *Extracted Effective Permittivity values in the frequency band of 50 MHz - 9 GHz from simulations and measurements.*

effective permittivity values a different distance to body and also in free space. On curve muscle measurement curve converges with the 10 µm air gap curve revealing the existence of thin film of air in the measurements. In the figure it can be observed the value of the effective permittivity varies from 1.3 in air to 6 on body measurements. Hence, the variance of proximity could affect the performance of the circuit significantly. Nevertheless, the air gap of 500 µm causes the effective permittivity curve to merge with the free space simulation and measurement curves. Therefore, if a distance of 0.5 mm is maintained from the body, the phase would not vacillate problematically.

6.1.6. Distributed Parameters

Figure 6.6. consists of rest of the distributed parameters. The parameters being (a) conductance per unit length (b) inductance per unit length and (c) capacitance per unit length. Conductance illustrates same information as the effective loss tangent that is the dielectric loss. The picture nevertheless enables to differentiate the transitions more

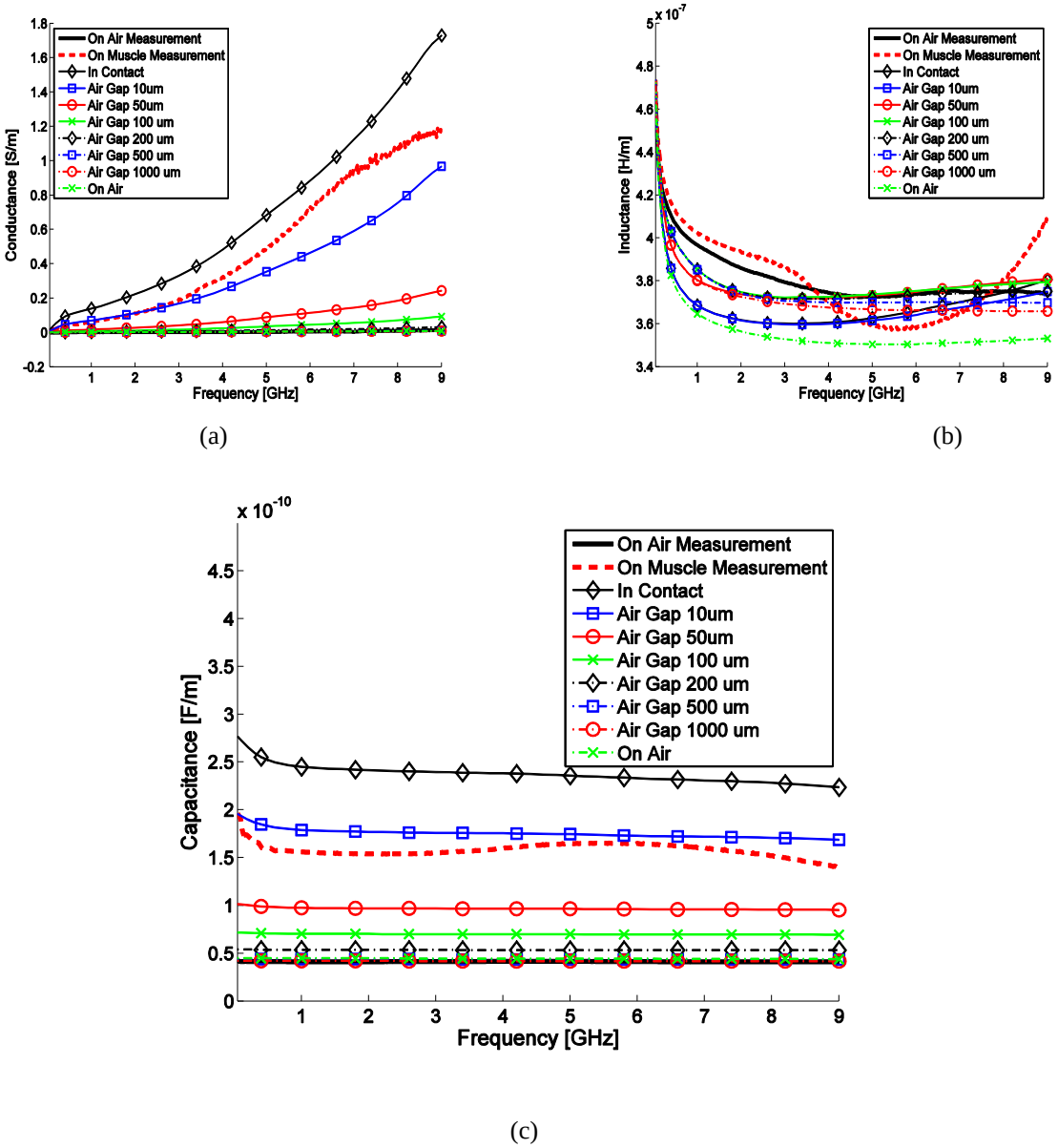

Figure 6.6. *Extracted (a.) Conductance (b.) Inductance (c.) Capacitance per unit length values in the frequency band of 50 MHz - 9 GHz from simulations and measurements.*

vividly. At 9 GHz the conductance increases from approximately 0 S/m to 1.73 S/m as the proximity of muscle is increased from free space measurement to on contact measurement. Conductance curve when the air gap is 0.5 mm approaches zero that is the dielectric starts to behave like an ideal dielectric. Figure 6.6. (b) and (c) shows how the magnetic and electric energy are stored in the RF interconnects, substrate and the muscle. The inductance and capacitance both increase as the muscle is brought closer to the CPW. The inductance increases in average from 0.26 μH/m to 0.37 μH/m that is approximately 42%. The capacitance increases from 44 pF/m to 175 pF/m that is around 300%. The phenomenon explains the decrease in the value of characteristic impedance. The expression of characteristic impedance is given in Section 3.5. Eq.(7).

6.2 Analysis of Substrate Thickness on RF Interconnects

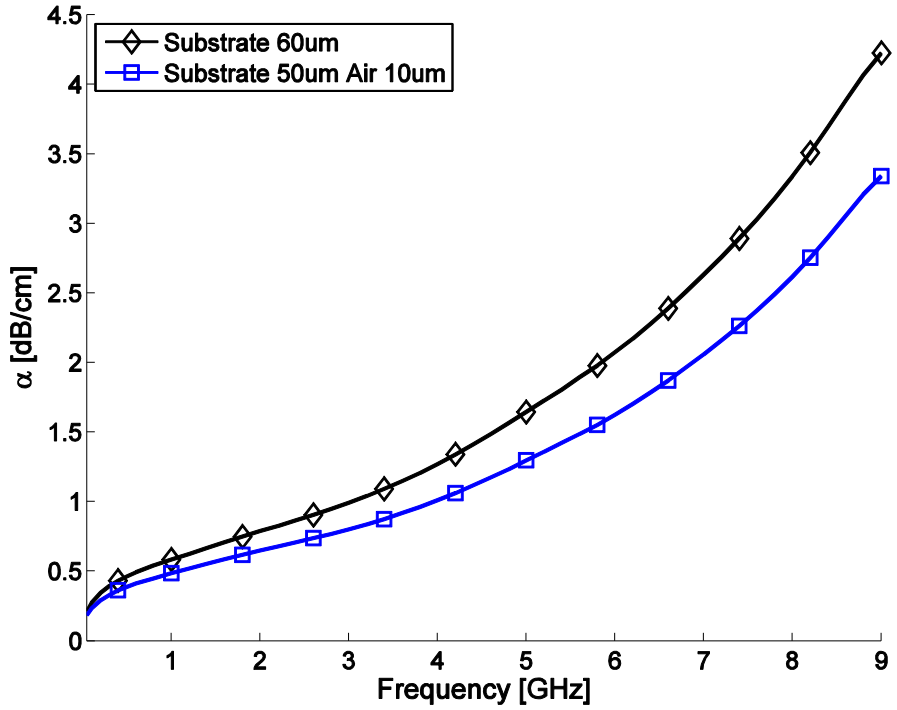

Figure 6.7. *Extracted Attenuation Constant per unit length values in the frequency band of 50 MHz - 9 GHz from simulations of varying substrate thickness in presence and absence of air gap keeping distance from the body 60 µm.*

In previous section it has already been shown, how the distance from muscle effects the parameters representing the characteristics of the RF interconnections. Building on the concept the objective of this section is to investigate how the distance from body occupied with air and PEN substrate differs in affecting the characteristics of the RF interconnects. Figure 6.7. shows the variation of attenuation constant value when the distance is 60 µm from the muscle. The figure consist of two simulations in one of the simulations the distance from the body is filled by 60 µm of PEN substrate and in the other the distance is filled with a 50 µm layer of PEN substrate followed by 10 µm layer of air. The curve with 60 µm of substrate incurs more loss than the 50 µm of substrate and 10 µm of air. The layered substrate incurs lower loss than homogenous substrate. Since, air is a better dielectric medium than the PEN substrate the fact that the simulation shows that the air film produces lower loss than substrate layer is justified. At 9 GHz the attenuation constant for 60 µm substrate is 1.44 dB/cm and the attenuation constant for 50 µm substrate and 10 µm air gap is 0.95 dB/cm. The attenuation constant decreases by 34% because of replacing the 10 µm of substrate with 10 µm of air. How the losses are distributed in conductor and in dielectric can be discerned from Figure 6.8.

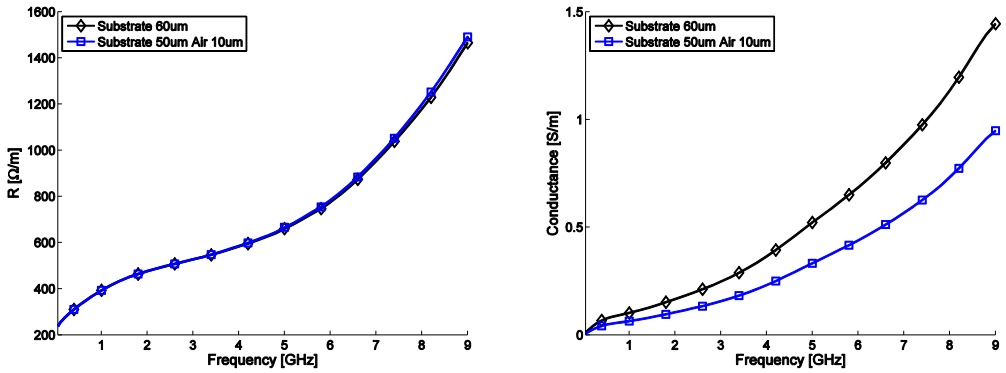

(a) (b)

Figure 6.8*. Extracted (a) Resistance per unit length and (b) Conductance per unit length values in the frequency band of 50 MHz - 9 GHz from simulations of varying substrate thickness in presence and absence of air gap keeping distance from the body 60 µm.*

The attenuation constant is the sum of dielectric loss and conductor loss. Therefore, Figure 6.8. (a.) and 6.8. (b.) would be able to illustrate how the losses are distributed in the conductors and the dielectric. Figure 6.8. (a.) shows that the curves of resistance per unit values for in contact and air gap simulations merges with one another. The resistance per unit basically as have already mentioned represents the conductor loss. The power loss in a conductor is a function of skin effect surface resistance and the current density. The skin effect surface resistance depends on conductivity and frequency. The current density depends on width of the conductor and the conductor thickness. Since, the conductor conductivity and the dimensions of the CPW are the same the conductor loss should be the same as well. The steep rise in the conductor loss after 5 GHz is a loss that is reflected due to the muscle. The muscle can acts as a lossy ground plane that is absorbing the energy that is reflected in the conductor loss. In this particular situation depicted in Figure 6.8. (a.) the materials under the traces are same, thus, the conductor losses for both of the simulations are almost same. Nevertheless, above 5 GHz the resistance value for 10 µm air gap curve starts to increase marginally more than in contact simulation but the increase is not that significant. The resistance per unit length values for both of the simulations varies approximately from about 250 Ω/m to 1600 Ω/m.

In Figure 6.8. (b.) shows the variation of the conductance of the dielectric medium which in one of the simulations is composed of the PEN substrate and the muscle and in the other case is the PEN substrate, air and muscle. The conductance curve of the 60 µm substrate in contact to muscle simulation resides above the 50 µm substrate and 10 µm air filled simulation curve, depicting that the dielectric loss is more for the 60 µm substrate simulation. The increase in the dielectric loss can be seen in the attenuation constant. Thus, since the conductor losses for both the simulations are the

same the difference in attenuation constant per unit length in Figure 6.7. is due to the dielectric loss.

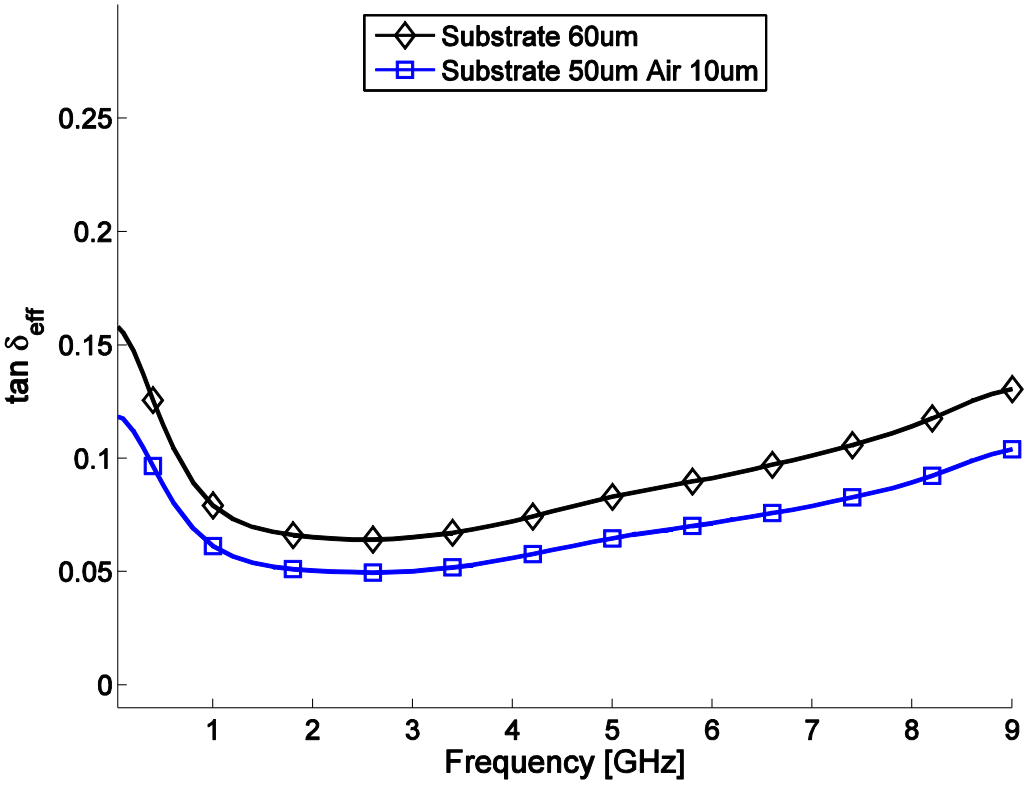

Figure 6.9. *Extracted Effective Loss Tangent values in the frequency band of 50 MHz - 9 GHz from simulations of varying substrate thickness in presence and absence of air gap keeping distance from the body 60 µm.*

Figure 6.9. shows the variation of effective loss tangent and the figure illustrates the same characteristics as the Figure 5.8.b. that is the dielectric loss. The effective loss tangent for the 60 µm substrate is greater than the 50 µm substrate. The values of effective loss tangent vary from 0.05 to 0.1 for the 50 µm and the values of effective loss tangent vary from 0.07 to 1.4. Thereby, the variation of effective loss tangent for the two simulations varies significantly. Figure 6.10. reflects the effect of muscle on the effective permittivity of the dielectric medium. Above 2 GHz the effective permittivity for the 50 µm substrate is 6.7 and for the 60 µm substrate is 7. The change is evident because the permittivity of the substrate is about three times the permittivity of the air and thereby the combination of PEN substrate and muscle should have a higher the effective permittivity compared the effective permittivity of substrate, air and muscle.

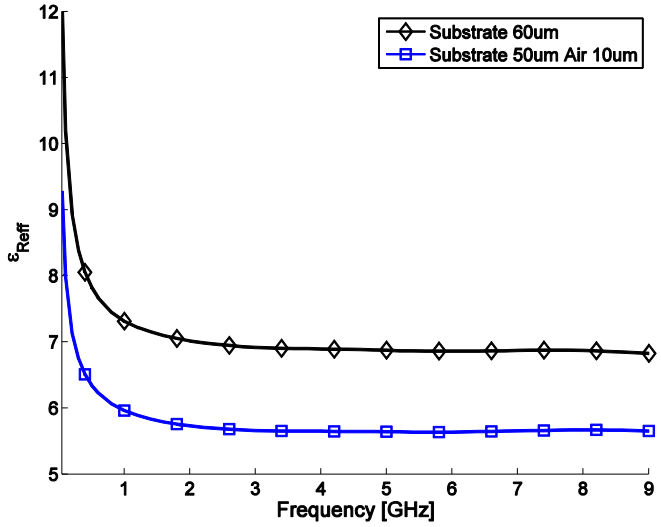

Figure 6.10. *Extracted Effective Permittivity values in the frequency band of 50 MHz - 9 GHz from simulations of varying substrate thickness in presence and absence of air gap keeping distance from the body 60 µm.*

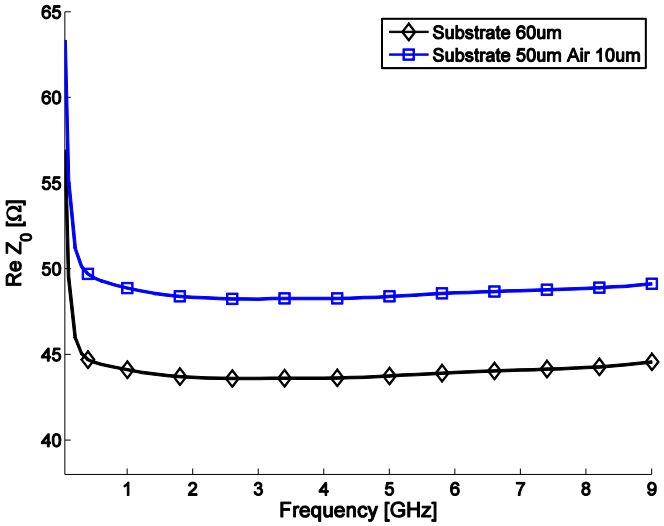

Figure 6.11. *Extracted Real part of Characteristic Impedance values in the frequency band 50 MHz - 9 GHz from simulations of varying substrate thickness in presence and absence of air gap keeping distance from the body 60 µm.*

The variation of real part of characteristic impedance provided in Figure 6.11. for varying substrate thickness. The value of the real part of characteristic impedance for 60 µm substrate in contact to muscle at 1 GHz is 44.11 Ω, at 5 GHz is 43.75 Ω and at 9 GHz is 44.58 Ω. Therefore, on average the real part of the characteristic impedance is 44 Ω. Similarly, the $R(Z_o)$ for the 50 µm substrate and 10 µm air gap is 48 Ω. The impedance value for air gap is higher compared to on muscle simulation.

6.2. Analysis of Dimension of RF Interconnects

The characteristics of a CPW changes because of varying the dimensions of the CPW and in this section the simulations results are utilized to attain certain guidelines for dimensions that would mitigate the effect of muscle on RF interconnects. The effect of altering dimensions on the losses and also the other characteristics of the interconnects are investigated. The section is divided in two parts. Section 6.2.1. illustrate the effect of varying gap width while keeping the trace width constant and Section 6.2.2. illustrates the effect of varying the trace width while keeping the gap width constant. The term gap is used to imply the gap between the signal and the ground conductor traces and the term trace is used to mean the centre line or in other word the signal trace that is used to transmit the signal through the CPW.

6.3.1. Variation of Gap

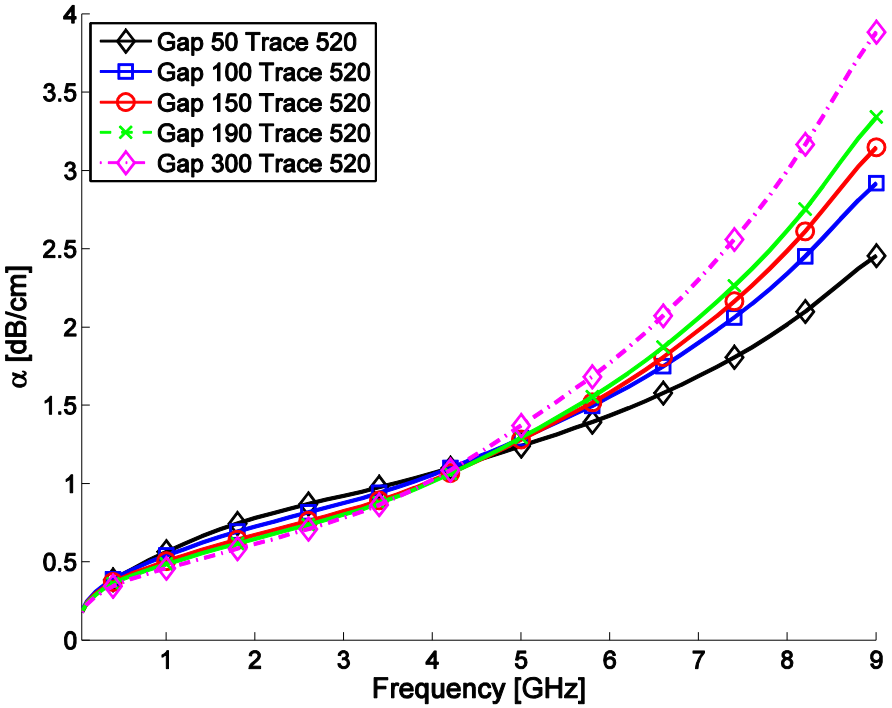

Figure 6.12. *Extracted Attenuation Constant values in the frequency band of 50 MHz - 9 GHz for varying gap width from simulations.*

Figure 6.12. displays the attenuation constant values for five different gap width of CPW in the frequency band of 50 MHz to 9 GHz. All the curves are simulation results. The gaps widths that are considered to be analyzed are 50 µm, 100 µm, 150 µm, 190 µm and 300 µm. 190 µm width is considered in simulation instead of 200 µm, which would have made the step uniform is because of the fabricated dimensions of the CPW on average are 190 µm. This gives the opportunity to compare the simulations

with measurements. The centre line width is also kept to 520 μm for the same reason. In all the simulations the 10 μm air gap is kept in order to emulate the measurements, which has already been deduced from the results in Section 6.1. From the curves a trend that can be observed is that with decreasing the width of the gaps the losses at lower frequencies (till 4.2 GHz) increases and at higher frequencies an opposite trend is observed that is as the gap is increased the losses increases as well. The reasoning for the phenomenon would be, when the gap width is narrower the conductor losses increases because the current density in the 520 μm centre line trace increases but as the gap width is wider the electric field (E) lines penetrates deeper in the muscle and the energy of the propagated signal is attenuated by the dielectric polarization and the conductivity in the muscle. All the curves intersect at approximately at a single point and the value of the frequency and the corresponding value of the attenuation constant is 4.2 GHz and 1.087 dB/cm respectively. The variations can be clarified further with the help of a table.

Table 6.5. *Attenuation Constant values at three different frequency points for gap width of 50 μm and 300 μm.*

Frequency / GHz	α (dB/cm) for 50 μm	α (dB/cm) for 300 μm
1	0.565	0.457
5	1.241	1.372
9	2.456	3.885

Table 6.5. shows the values of attenuation constant for two CPW of with gap width of 50 μm and 300 μm at three different frequency points. The two extreme gap width attenuation curves envelopes the other simulation curves. Hence, these two situations are utilized to illustrate the variations in the attenuation constant values. At 1 GHz the loss incurred for the 50 μm gap is 0.108 dB/cm more than the loss incurred for the 300 μm gap. The attenuation constant values for the 300 μm gap CPW starts to become more than 50-μm gap CPW as the frequency increases. Hence, at 2 GHz α (dB/cm) is 0.131 dB/cm greater than α (dB/cm) for the 300 μm gap width. α (dB/cm) becomes 1.427 dB/cm greater than α (dB/cm) of the 50 μm gap at 9 GHz. The difference at low frequency is only in the order of 0.1 dB/cm but as the frequency is increased the magnitude of the difference increases to 1.5 dB/cm. Therefore, judging from gap analysis it can be stated that for BWE applications narrower gap width should be used to mitigate the effect of muscle for frequencies above 4 GHz. The distribution losses can be further understood in observing R (Ω/m) and G (S/m).

In Figure 6.13. the resistance per unit length curve for the 50 μm gap is above rest of the curve till 5.4 GHz. The curve for the 50 μm reaches its maximum value at around 4 GHz and value at 4.2 GHz is 725 Ω/m and it remains constant for the rest of the frequency range. Hence, when the gap is made narrower the effect of the muscle acting as a lossy ground plane increasing the conductor loss above 5 GHz can be neglected. However, decreasing the gap increases the current density in the edges of the centre line

and thus, increases the conductor loss below 5 GHz. Increasing the gap on the other hand has an opposite effect as depicted by the 300 µm gap curve. At 9 GHz the value for *R* (Ω/m) for the 50 µm gap is 765 Ω/m and for 300 µm gap is 2074 Ω/m. The resistance value increases 1.7 times consequently multiplying the conductor loss by the same factor.

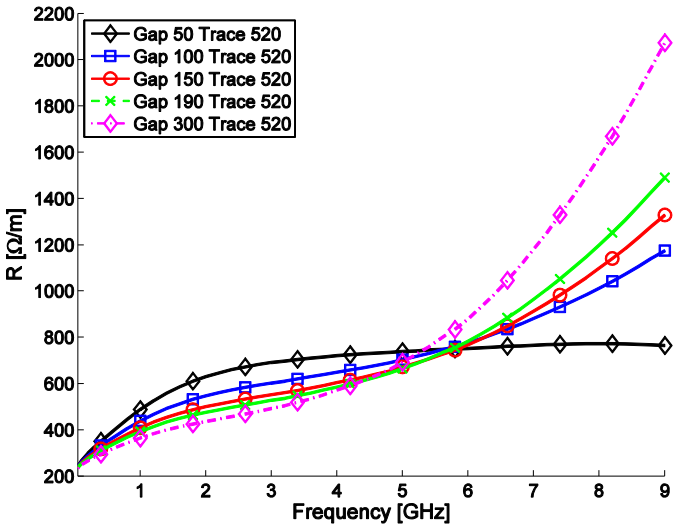

Figure 6.13. *Extracted Resistance per unit length values in the frequency band of 50 MHz - 9 GHz for varying gap of CPW from simulations.*

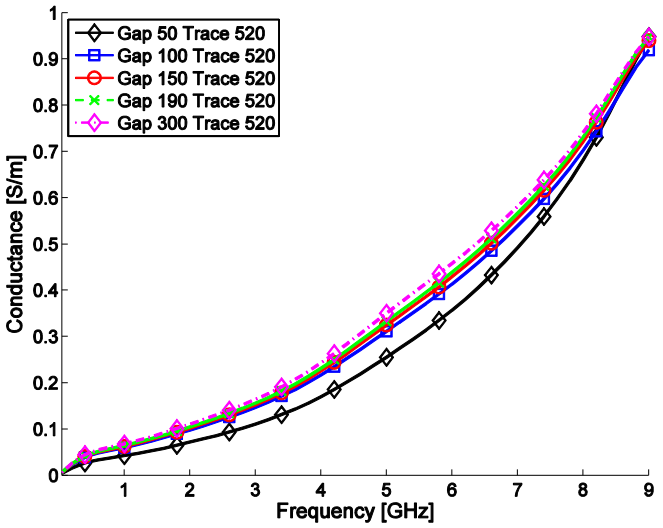

Figure 6.14. *Extracted Conductance per unit length values in the frequency band of 50 MHz - 9 GHz for varying gap of CPW from simulations.*

The variation of conductance for varying gap width of CPW is illustrated in Figure 6.14. The conductance also represents dielectric loss and from the Figure 6.14. it

can be observed that dielectric loss is the lowest for the narrowest gap (50 µm) width considered in the simulations. The curve for 300 µm lies above all the curves, thereby, revealing that the largest gap incurs the highest dielectric loss. The curve for the 50 µm gap coincides with the 300 µm at 9 GHz and judging from the trend of the curves there could be a possibility that at higher frequency the dielectric loss for 50 µm could be more than 300 µm gap. The conductance value at 5 GHz for 50 µm gap is 0.25 S/m and the value for 300 µm gap is 0.35 S/m and this is approximately the maximum deviation of conductance that occurs. Therefore, rise in the attenuation constant value in Figure 6.12. is mostly because of the increase in the conductor loss that occurs due to the muscle acting as a lossy ground place. The effect even though is because of the dielectric but is reflected in the resistance per unit length curves as shown in Figure 6.14.

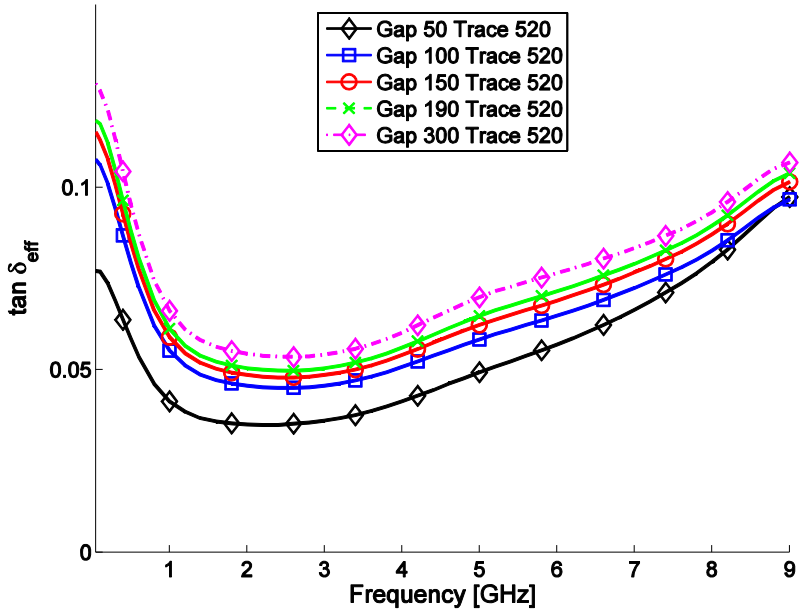

Figure 6.15. *Extracted Effective Loss Tangent values in the frequency band of 50 MHz - 9 GHz for varying gap of CPW from simulations.*

Another method of understanding the dielectric loss is by observing the effective loss tangent. The variation of the dielectric loss due to the variation of gap width of the CPW can be further illustrated using Figure 6.15. The $tan\delta_{eff}$ values at frequencies 1 GHz, 5 GHz and 9 GHz for 50 µm gap width are 0.041, 0.049 and 0.096 respectively. Apart from the 50 µm curve the other four curves for the wider gaps lies very close to one another. The highest $tan\delta_{eff}$ value at each frequency points, as already inferred from the conductance curves, are provided by the 300 µm gap. As the gap is increased from 50 µm to 100 µm the $tan\delta_{eff}$ increases to 0.055 at 1 GHz. However, the slope of the $tan\delta_{eff}$ due to 50 µm gap is much greater than rest of the curves as a consequence of which the $tan\delta_{eff}$ of the 50 µm gap intersects the curve of the 100 µm gap at 8.8 GHz. For the 300 µm at 1 GHz the $tan\delta_{eff}$ value is 0.066, at 5 GHz the value is 0.069 and at

9 GHz the value increases to 0.107. Nevertheless, the statement needs to be recalled that even though the 50 µm provides the lowest dielectric in the frequency band of 50 MHz to 9 GHz but judging by the slope of $tan\delta_{eff}$ of 50 µm gap the dielectric losses a higher frequencies could be greater.

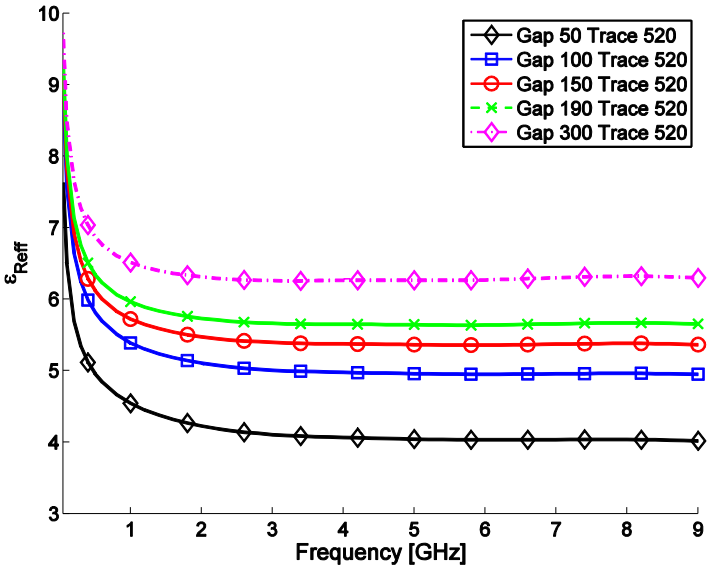

Figure 6.16. *Extracted Effective Permittivity values in the frequency band of 50 MHz - 9 GHz for varying gap of CPW from simulations.*

Increasing the gap of the CPW increases the effective permittivity of the transmission line as illustrated by Figure 6.16. At 5GHz the ε_{reff} value for different gap width is as follows: at 50 µm is 4.04, at 100 µm the value of ε_{reff} is 4.96, at 150 µm the value of ε_{reff} is 5.36, at 190 µm the value of ε_{reff} is 5.64 and at 300 µm the value of ε_{reff} is 6.27. The values could be useful for obtaining the electrical length (βl) of the RF interconnects.

The real part of the characteristic impedance increases with increasing gap as displayed in Figure 6.17. The real part of the characteristic impedance of the 50 µm gap curve tends to decrease with increasing frequency which in fact is an anomaly compared to the other four simulation results for the wider gap widths. Since, the slope of $Re[Z_o]$ for gaps greater than 50 µm is constant, selecting a value of $Re[Z_o]$ at any frequency should be enough to provide value of $Re[Z_o]$ at the larger gap widths. At 5 GHz the values of $Re[Z_o]$ at varying air gap are 43.74 Ω [100 µm], 46.59 Ω [150 µm], 48.39 Ω [190 µm] and 52.24 Ω [300 µm]. When the gap width is 50 µm the $Re[Z_o]$ value at 1 GHz is 43.81 Ω, at 3.4 GHz is 41.34 Ω, at 5 GHz is 40.64 Ω, and at 9 GHz is 38.83 Ω. The decrease in the characteristic impedance could be understood from the variation of the distributed parameter that is the capacitance that starts to increase as the frequency increases.

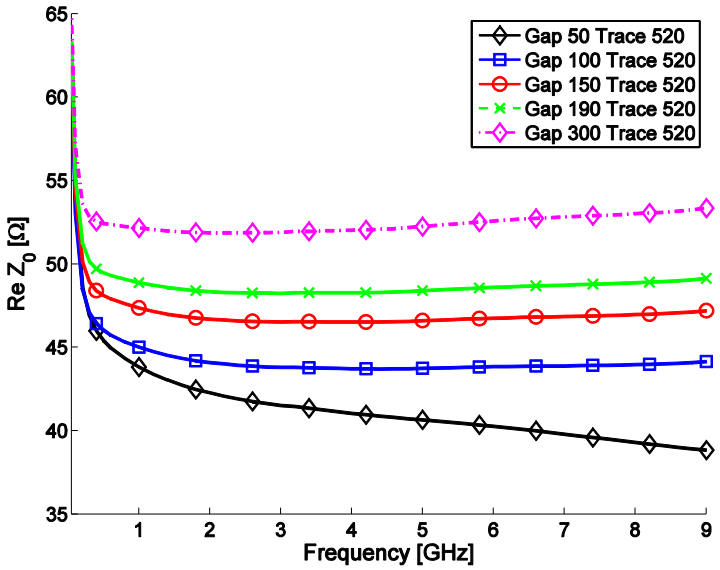

Figure 6.17. *Extracted Real part of Characteristic Impedance values in the frequency band of 50 MHz - 9 GHz for varying gap of CPW from simulations.*

At frequencies lower than 4.2 GHz the conductor losses dominates and the narrow gap causes the conductor loss to increase. However, the effect of muscle becomes predominant at frequencies greater than 4.2 GHz. The dielectric losses start to contribute more to the total loss which significantly increases the total loss for the CPW of gap width greater than 50 µm. To summarize, for frequency less than 4.2 GHz, using wider gap width is beneficial because the conductor losses are less and the attenuation constant values are less as well. But in order to nullify the effect of muscle in the conductor loss at higher frequencies narrow gap in the order of 50 µm should be used. Therefore, the gap width that should be adopted is frequency dependent.

6.3.2. Variation of Centre Line

In Figure 6.18. all the curves are values of α *(dB/cm)* obtained from simulations. In the simulations the gaps are all 190 µm but the width of the centre line is varied. α (dB/cm) for the 100 µm width centre line trace is the highest among the five width analysis at lower frequencies lower than 4 GHz. At 1GHz the value of α (dB/cm) for 100-µm is 0.67 dB/cm while for the other four curves values all converge to value about 0.49 dB/cm. α (dB/cm) for 300 µm, 400 µm, 520 µm and 600 µm centre line width lies very close to one another till 3 GHz. Thus, the CPWs except for center lines narrower than 100 µm, have similar losses at lower frequencies but with increasing frequency the

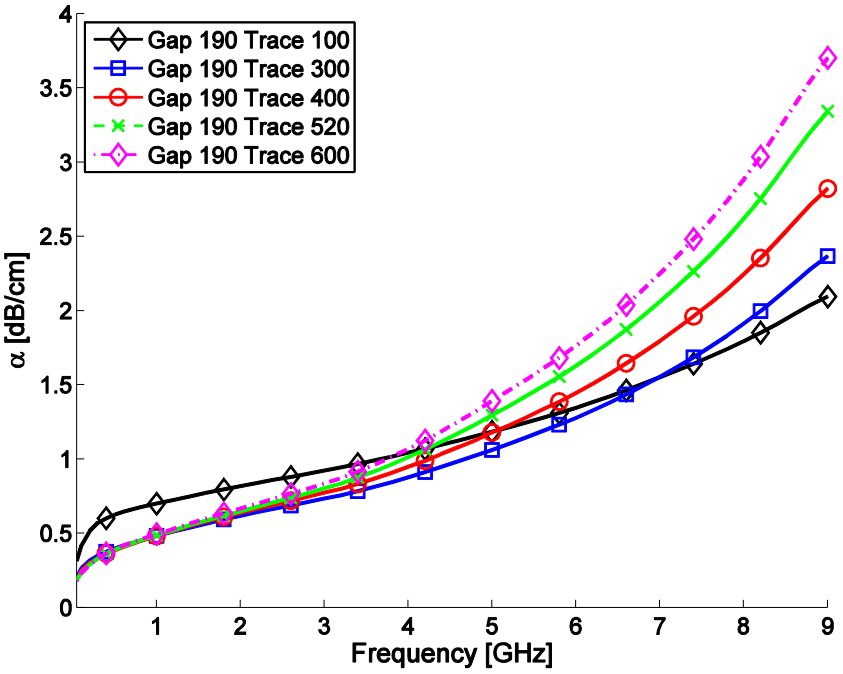

Figure 6.18. *Extracted Attenuation Constant values in the frequency band of 50 MHz - 9 GHz for varying centre line width from simulations.*

losses starts to diverge. The curves start to diverge significantly after 4 GHz. Therefore, at frequencies lower than 3 GHz if the CPW interconnects width are not made as narrow as 100 µm then the choice of value of width to be used depends on the desired impedance. Narrowing the width increases the current density on the edges of the centre line, thus, increasing the conductor losses. The difference of the attenuation constant α could be better expressed with a table.

Table 6.6. *Attenuation Constant per unit length value (α dB/cm) value at 9 GHz for varying width of centre line of CPW.*

Width of Centre line (µm)	100	300	400	520	600
α (dB/cm)	2.09	2.36	2.82	3.34	3.70

Table 6.6. shows the gradual change of attenuation constant per unit length value at 9 GHz. Therefore, at 9 GHz the narrowest trace width has the lowest loss and the widest trace has the largest loss. Thus, at higher frequency it is a better choice to use narrow width for centre line of CPW for BWE applications. The rise in the loss is because of the dielectric loss that is superseding the increase in conductor loss due to the narrow gap. The situation could be better deduced with the resistance per unit length and conductance per unit length figures.

Table 6.7. *Resistance per unit length value (Ω/m) value at 1 GHz and 9 GHz for varying width of centre line of CPW.*

Width of Centre line (μm)	100	300	400	520	600
R (Ω/m) at 1 GHz	1260	557.7	466.1	393.3	362.7
R (Ω/m) at 9 GHz	1890	1377	1414	1491	1593

Values in Table 6.7. have been taken from Figure 6.19. For 100 μm trace width the current distribution starts to concentrate at the edges of the conductor increasing *R* (Ω/m) significantly, when compared to the other four simulation results. The closest to the curves to the 100 μm curve at 1 GHz is the curve for 300 μm. Even though 300 μm is the second narrowest line yet the difference in the values is above 50 %. The 600 μm line produces the lowest. From Figure 6.19. 100 μm line starts from the a very high value but the variation

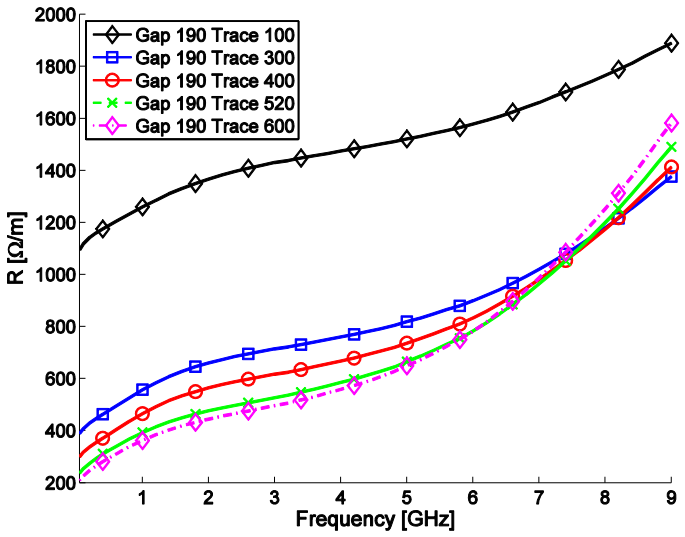

Figure 6.19. *Extracted Attenuation Constant values in the frequency band of 50 MHz - 9 GHz for varying centre line width from simulations.*

in the value of *R* (Ω/m) in the frequency band of 1 GHz to 9 GHz is lower (630 Ω/m) compared to the other for four curves, for instance, for the 600 μm the variation in the same frequency band is 1231.3 Ω/m. The effect of the muscle acting as a lossy ground plane is more significant in the wider centre line CPW compared to the narrower line.

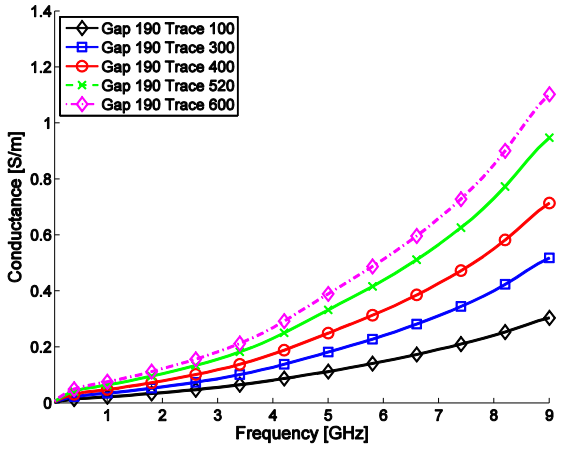

Figure 6.20. *Extracted Conductance values in the frequency band of 50 MHz - 9 GHz for varying centre line width from simulations.*

Figure 6.20. shows the variation of the conductance value for varying centre line width. The dielectric loss that can be deduced from the variation of the conductance curves illustrates that the dielectric loss for the widest centerline is largest (at 9 GHz is 1.2 [S/m]) and is the lowest for the narrowest centre line is the lowest (at 9 GHz is 0.32 [S/m]). Figure 6.21. illustrates the variation of $tan\delta_{eff}$ for the varying width of the centre line. With increasing trace width $tan\delta_{eff}$ values increases and in other words, the dielectric losses increases as well. The curves of the narrowest and the widest trace width envelopes the other simulation curves. For 100 µm trace width the $tan\delta_{eff}$ value varies from 0.043 (1 GHz) to 0.067 (9 GHz) and for 600 µm the $tan\delta_{eff}$ varies from 0.065 (1 GHz) to 0.0117 (9 GHz).

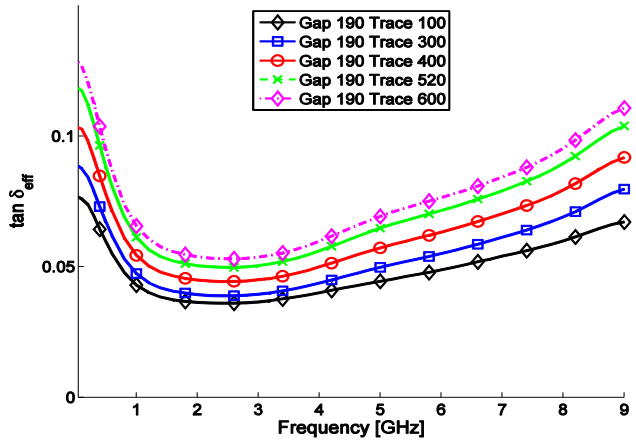

Figure 6.21.*Extracted Effective Loss Tangent values in the frequency band of 50 MHz - 9 GHz for varying centre line width from simulations.*

Figure 6.22. and Figure 6.23. shows the effective permittivity and real part of characteristic impedance respectively. The value of effective permittivity and real part of characteristic is important for RF design because it enables to determine the electrical length of the transmission line and attain matching of impedance in RF circuitries. For both the figures the values are very constant in the frequency band of 1 GHz to 9 GHz. Table 6.6. provides the average value of effective permittivity and real part of characteristic impedance.

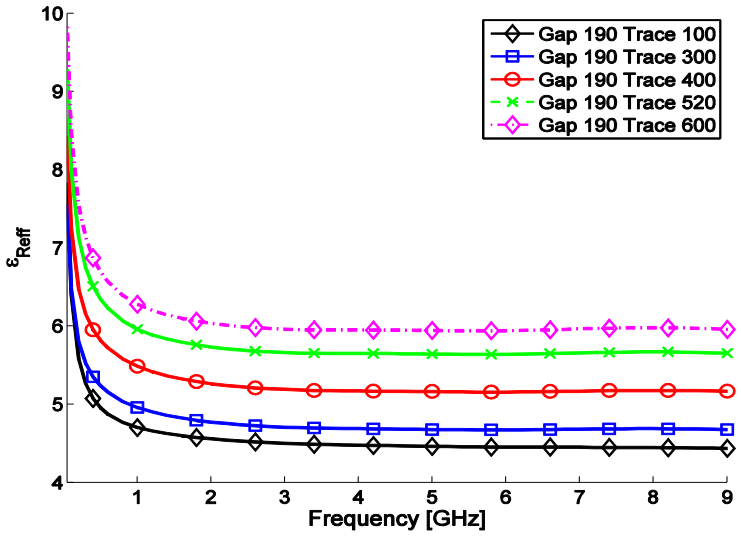

Figure 6.22. *Extracted Effective Permittivity values in the frequency band of 50 MHz - 9 GHz for varying centre line width from simulations.*

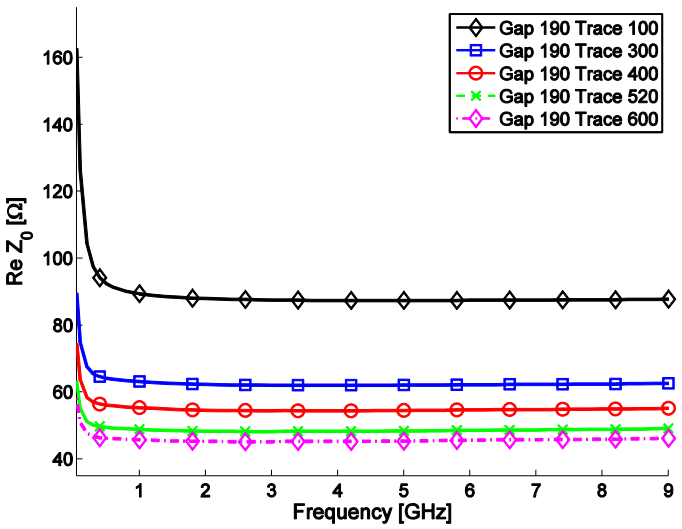

Figure 6.23. *Extracted Real part of Characteristic Impedance values in the frequency band of 50MHz - 9GHz for varying centre line width from simulations.*

Table 6.8. *Effective Permittivity and Real part of Characteristic Impedance values for varying width of the centre line of CPW.*

Width of Centre line (μm)	100	300	400	520	600
ε_{reff}	4.462	4.678	5.161	5.642	5.944
$Re[Z_o]$ (Ω)	87.40	62.09	54.53	48.39	45.39

For BWE the width of the centre line should be made wider at frequencies lower than 4 GHz in order to decrease the conductor losses which contribute more to the total loss before 4 GHz. For frequencies greater than 4 GHz the design should adopt narrower centre line because the dielectric loss surpass the conductor loss with increasing frequency.

6.3. Bend Analysis

In BWE if the RF circuitries are made flexible the probability of bend occurring due the movements or due the contour of the body is very high. Therefore, to analysis the effect of bending is necessary. The following section pursues to illustrate the investigation. The investigation stands on the hypothesis that if bends does not affect the operation of CPW in air it should not affect the CPW performance when held close to the human body.

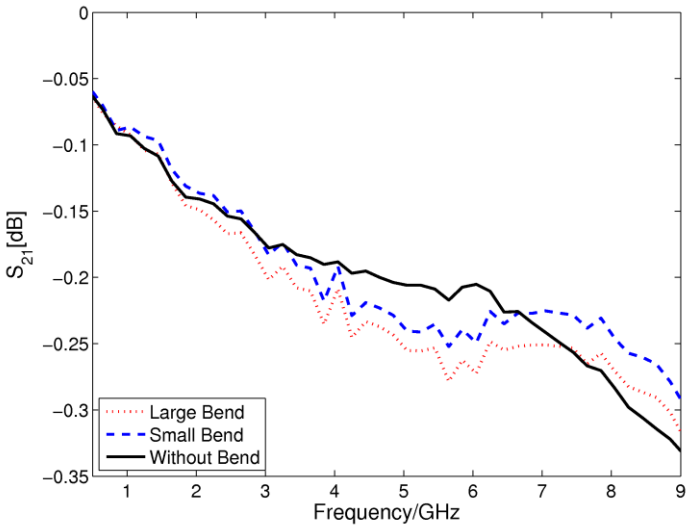

Figure 6.24. *S21 values from measurement of CPW of length 19 mm with 1.2 mm bend, 4 mm bend and without bend in the frequency band 50 MHz - 9 GHz.*

Figure 6.24. shows three measurement results that have been obtained from measuring a 19 mm CPW transmission line on microwave air foam. The measurements

have been performed to understand the effect of bending on interconnects. Hence, to undertake the investigation a transmission without bend is measured on low loss microwave air foam. After that being done two other measurements with 1.2 mm and 4 mm bend diameter have been performed with the same transmission line. The bends are produced with same microwave foam in which the measurements are taken to emulate free space measurement. In the Figure 6.24. it is observed that the curves lie at close proximity to one another, however, there is some divergence at varying frequencies. Pronounced divergence is observed at 5.25 GHz between bend transmission line curves and without bend transmission curve. The order of divergence is about 0.04 dB. The average maximum divergence between the bend lines is 0.03 dB. The variations are not large enough to affect the performances of a circuit significantly. The bend lines were measured with the same calibrations and the without bend 19 mm line was measured with a different calibration and this could very well cause the variations in the results. The variations in bend line measurements are similar to one another while the variations in the straight line are different this could be caused because of the different calibrations. Hence, it cannot be concluded with certainty whether the variations are because of the bends. However, the difference of bend diameter did not cause much of a change in S21 curves.

Figure 6.25. (a.) and Figure 6.25. (b.) displays the results for CPW transmission lines of length 25 mm and 31 mm respectively. The results are provided to verify and validate the conclusions derived from Figure 5.24. The average maximum deviations obtained

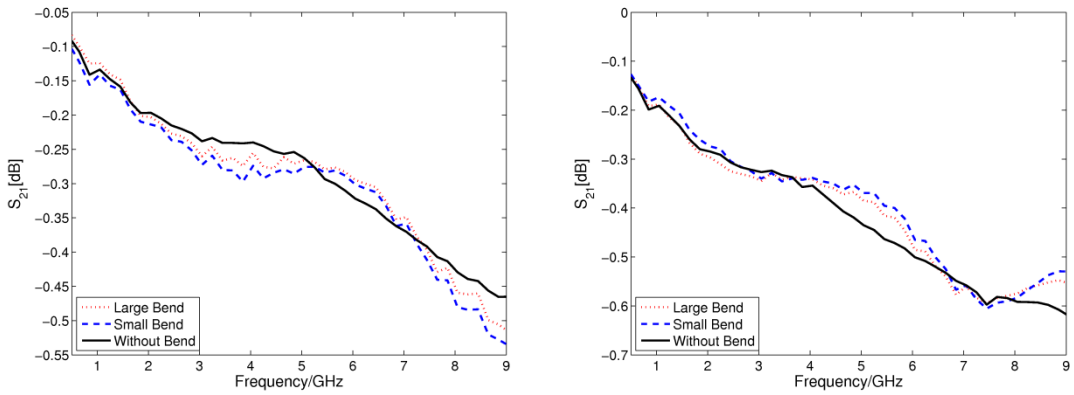

(a.) (b.)

Figure 6.25. *(a.) S21 values from measurement of CPW of length 25 mm (b.) S21 values from measurement of CPW of length 31 m, with 1.2 mm bend, 4 mm bend and without bend in the frequency band 50 MHz – 9 GHz.*

between the bend and without bend transmission lines of length 25mm and 31 mm are around 0.08 dB and 0.14 dB respectively. The bend transmission line curves in both Figure 6.25. (a.) and Figure 6.25. (b.) do not vary more than 0.02 dB. Hence, in conclusion from the analysis of the measurements, variations are observed between the bend and without bend measurements. The variation could possibly be due to

calibration but the variation is in the order of 0.1 dB. Therefore, since the difference in transmission parameter of the bend and straight lines are not significant, the bends does not affect on the performance of RF interconnects significantly in the observed frequency band.

6.5. Filter Analysis

Since transmission line simulations and measurements complied with one another, the findings create the foundation for the investigations to be proceeded to analysis the effect of muscle on RF circuits. In this section body effects on discrete RF circuits is investigated. The filter used as test structures and simulation model are described in Section 5.2. In the Section the simulations and measurements for the filter structures would be compared. The components used to construct the low pass filters are inductors of HK1005 multilayer structures from Taiyo Yuden and capacitors are C1005COG series multilayer capacitors from TDK. Due to the disagreement between the measurements and simulation results particularly in the stop band, possible reasons for the disagreements were pondered. Consequently, experiments where performed and the experiments revealed that filters constructed on FR4 substrate provided a better match with simulations. The findings pointed towards the possibility that the disagreement could be due to scattering parameters of the components that are used in the simulations which are obtained from measuring components on FR4 substrate. The measurements in the research are being performed on 50-µm PEN substrate which is quite different from the FR4 substrate both in regard of its thickness and material composition. Hence, a new method is adopted in which scattering parameters of each of components on microwave air foam and on muscle is calculated by de-embedding the error boxes from both ends. The multiline TRL error boxes are used [11]. And the investigation of filter analysis involves the comparison of filter simulations using the AWR components and also the measured components.

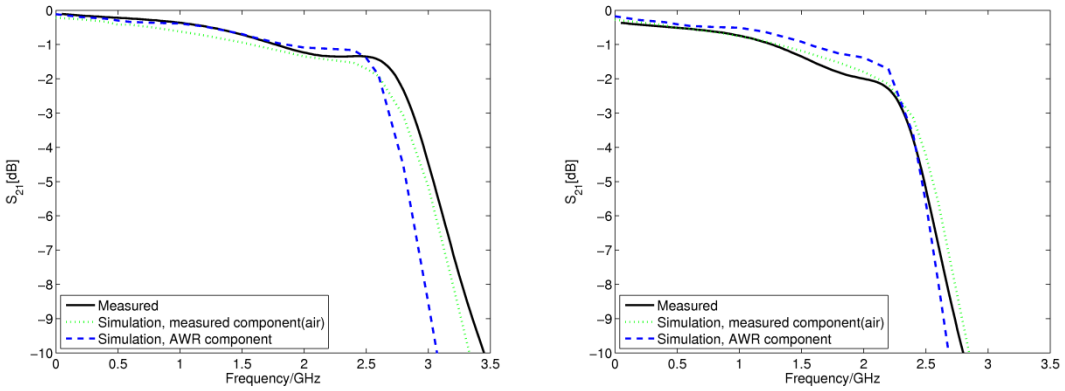

Figure 6.26. *(a.) Small filter free space simulation and measurement results (b.) Larger filter free space simulation and measurement results.*

Figure 6.26. shows the simulation and measurement results of filters on low loss microwave foam. Figure 6.26. (a.) is the simulation and measurement curves of the small filter of length 6 mm and Figure 6.26. (b.) are the results of the larger filter of length 14 mm. For the small filter in the pass band the filter consisting of the AWR components follows the measured curve till 1.8 GHz and difference between the measurement curve and measured component curve is about 0.25 dB. One of the important parameter is the 3 dB bandwidth of the low pass filter. The 3 dB value is reached at 2.86 GHz, 2.80 GHz and 2.62 GHz for the measured, measured component and AWR component simulation curves respectively. Even though the AWR components provides a decent match at low frequency but there is about 0.26 GHz difference between estimated 3 dB bandwidth of AWR component simulation and measured filter. However, the difference in the estimation between the measurement and measured component simulation is only 0.06 GHz. The opposite trend is observed in the larger filter free space emulated measurement and simulation curves shown in Figure 6.26. (b.). The measured component curve converges well in the pass band with the measurement curve till 1.3 GHz but at the cut off frequency that is when S21 values decreases by 3 dB the curve of simulation performed with AWR components converges with the measurement curve at 2.33 GHz. The measured components curve over estimates the cut off frequency to be 2.4 GHz. The measured components proved to be more useful for small filter compared to the larger filter but the divergence from the actual value is about 70 MHz.

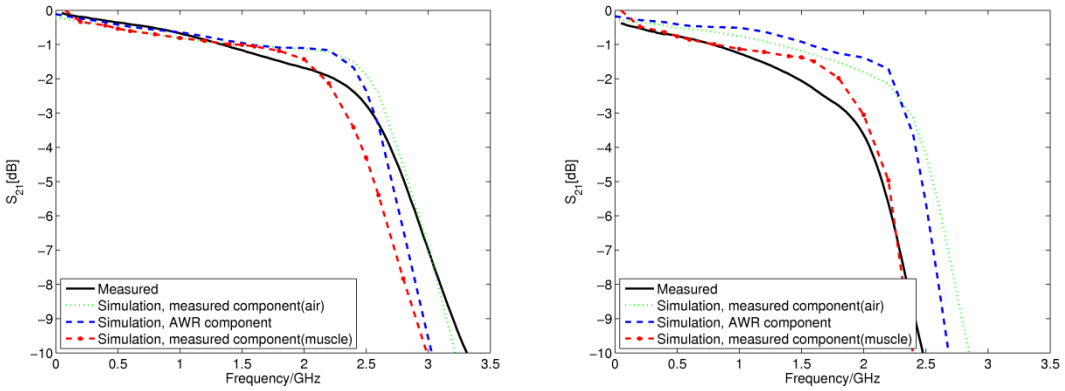

Figure 6.27. *(a.) Small filter on muscle simulation and measurement results (b.) Larger filter on muscle simulation and measurement results.*

Figure 6.27. shows the results of on muscle simulations and measurements. The figures consist of four curves that are composed of three simulation results and one measurement result. The three simulation results consist of AWR component simulations, components measured in microwave air foam and components measured on muscle. The small filter results shown in Figure 6.27. (a.) illustrate that the simulation performed with the on AWR components shows good agreement with the

measured curve until 1.3 GHz but as the frequency increases all the simulation curves except for the on muscle measured component curves underestimates the losses. The cut off frequency of the AWR component simulation curve and the measured curve coincides at 2.56 GHz. The on air foam measured component simulation curve estimates the cut off frequency to be at 2.66 GHz and the worst estimation of cut off frequency is provided by the on muscle component simulation curve; the value being 2.37 GHz. The point that needs to be highlighted is that the introduction of muscle caused the cut off frequency to decrease from 2.86 GHz to 2.56 GHz, that is, about 300MHz decrease. Therefore, for BWE applications the shift of platform on which an RF circuit is placed, could change the operating frequency of the circuit significantly.

Figure 6.27. (b.) shows the larger filter on muscle simulations and measurement results. In Figure 6.27. (b.) the simulation with the muscle measured components provides the best match with the measurement curve both in the pass band and stop band. On the contrary simulations with the AWR components and the air foam measured components underestimates the losses both in the pass band and the stop band. From the Figure 6.27. a conclusion can be deduced that the library components in FR4 substrate have different characteristics than the components in the thin substrate especially when brought very close to body. From the transmission line simulations and measurement results it has been deduced that significant loss is incurred because of the proximity of muscle but the decrease in cut off frequency is not entirely due to losses in the interconnections but also due the change in the value of the inductance and capacitance. Therefore, care needs to taken when designing on body RF circuits.

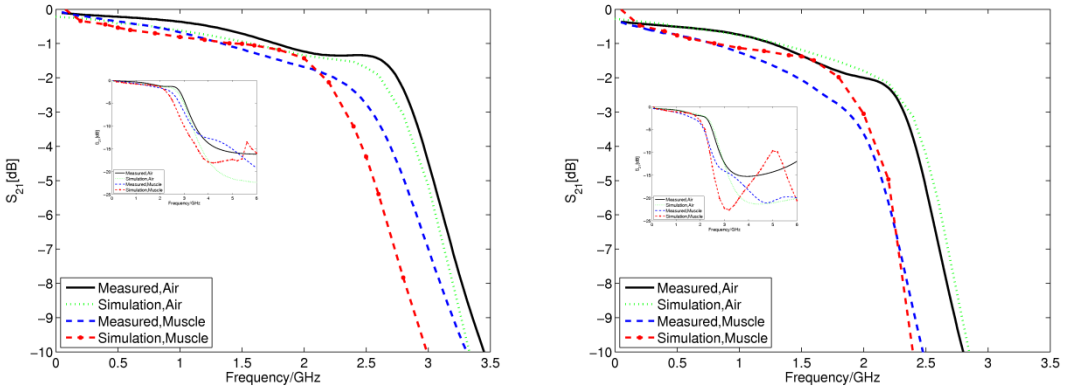

Figure 6.28. *(a.) Small filter simulation and measured in air and on muscle. Inset: Wideband results (b.) Larger filter simulation and measured in air and on muscle. Inset: Wideband results.*

Figure 6.28. (a.) and Figure 6.28. (b.) shows the on muscle simulations and measurement results of the small and the large filter respectively. The simulations for air are performed with air components and the simulations for muscle are with muscle components. The cut off frequency in the measurements decreases by 307 MHz and

430 MHz due the effect of muscle for the small and large filters respectively. 8 mm change of length in the filter affected the cut off frequency to change by 127 MHz. Hence, to mitigate the effect of muscle in RF circuits the design needs to be compact. Both the figures consist of the sub figures of same simulation and measurement results with frequency axis extended to 6 GHz. The variation in the initial stage of pass band for both filter structures the variations in the values of measurements and simulations are less than 0.5 dB. The sub figures are provided to compare the agreement of the simulation and measurement results at higher frequencies. From the inset figures it can be observed all the simulation results overestimates the losses at frequency above 3.5 GHz. Anomaly being the simulations results with the muscle components but that could be because of inaccuracy in the on muscle measurements at higher frequencies.

7. CONCLUSION

Prior to judge the achievement of the research the basic aims of the study require to be restated. The research aimed to attain a method of simulation that would be able accurately estimate losses incurred, when RF circuits are placed at close proximity to the body. Fresh beef was intended to emulate human muscle in measurements. The research also intended to discern how the losses were distributed between the dielectric and the conductor of the RF interconnects. Multiline TRL error box was solved to attain scattering parameters for discrete components in order to investigate whether the muscle and substrate affected the value of discrete components.

The simulations and measurements performed in the frequency band of 50 MHz to 9 GHz, agreed with one another for the RF interconnections hence, validating that AWR Microwave Office commercial software can be used for performing on muscle simulations. The mutiline extraction technique was able provide better insight to the obtained results and the dielectric loss was separated from the conductor loss. Essential parameters such as the effective loss tangent, effective permittivity, real part of characteristic impedance and the distributed parameters where successfully extracted using the multiline extraction method as well. The success of simulation because of its agreements with the measurements also opens the window for investigating the effect of human body on numerous RF circuits that requires to be placed close to human body.

The simulations reveal that a distance of 0.5 mm from the body, there is virtually no effect of the body on the RF interconnections and loss incurred becomes very close to that of free space. Nevertheless, the effect of muscle when in contact with RF interconnects significantly alters the characteristics of the RF interconnects. The increased loss, changes in the characteristic impedance and phase shift significantly distorts the performance of the RF interconnects. From the simulations it was deduced that wide signal trace and wide gap between the signal trace and ground traces should be used at frequencies below 4 GHz. While at higher frequency of operation narrow centre line width and gap should be used in RF circuits because it was found narrowing the gap mitigates the effect of muscle at higher frequencies. Measurements revealed that the bend does not have a significant effect on the performance of RF interconnects within the frequency band of investigation.

The validity of the RF interconnects measurement and simulation technique provided the foundation for the research to be extended to observe the effect of body on discrete components and simple RF circuits. The effect of the body was observed through measurements and simulations. The body has significant effect on the values of discrete components. The change of the component values together with the attenuation in the pass band caused the cut off frequencies for the low pass filters considered to decrease. The effect becomes more pronounced with increasing size of the filter. Multiline calibration has also been used to attain the scattering parameters of the components. The commercial RF simulator was successfully able to estimate the losses.

The results are valuable for body worn RF design were the additional loss and alteration of the operating frequency such as in antenna feeding network needs to taken into account accurately. Hence, for body worn circuits it is essential to take account of the losses due to the effect the body since, it has considerable effect in the performance of the circuit.

REFERENCES

[1] Johanson, A., Karlsson, A., Scanlon,W., Evans, N., Rahmat S. Y., "Medical implant communication systems," *in Antennas and Propagation for body-centric wireless communications,* 2nd ed., P.S. Hall and Y.Hao, eds, Artech House, ch. 9 pp.325-357, 2012.

[2] Kellomäki, T., " Effects of the human body on single-layer wearable antennas," *PhD thesis,* Tampere University of Technology, Tampere, 2012.

[3] Hall, P. S., Hao, Y., "Antennas and propagation for body-centric wireless communications," Artech House, London, 2006.

[4] Singh M., Haverinen H. M., Dhagat P., Jabbour G. E., "Inkjet printing-process and its applications," *Advanced materials.* vol. 22, no. 6. pp. 673-685, Feb. 2010.

[5] Sillanpää H., Rasku A., Mäkinen R., "A multiline material parameter extraction method," *Proc. 10th Mediterranean Microwave Symp.,* Guzelyurt, Cyprus, pp. 314-317, Aug. 2010.

[6] *AWR Microwave Office,* AWR Corporation: http://www.awrcorp.com/; referred Oct. 1, 2012.

[7] *Dielectric properties of body tissues* http://niremf.ifac.cnr.it/tissprop/; referred Oct. 1, 2012.

[8] Rasku, A., Sillanpää, H., Hiltunen, I., Mäkinen, R., "Multiline material parameter extraction method performance analysis," *Proc. Asia/Pacific Microwave Conf.,* Yokohama, Japan, 1905-1908, Dec.2010.

[9] Mäkinen, R., Rasku, A., Sillanpää, H., "Modeling-based printed electronics characterization," *Proc. IEEE Antennas Propaga. Intl. Symp.,* Chicago, IL,2p., Jul. 2012.

[10] Marks, R. B., "A multiline method of network analyzer calibration," *IEEE Trans. Microwave Theory Tech.,* Vol.39, No.7, 1205-1215, 1991.

[11] *Design of a Wearable Electronics Package for Firefighter Monitoring* Presentations on Electronics in PPE: http://www.cpe.vt.edu/appe/TuesAgenda.pdf; refered Oct. 1, 2012.

[12] *Mobile healthcare solutions,* Health Service 24 Project: http://www.healthservice24.com/; refered July 12, 2013.

[13] Bianying S., Wolf K. H., Gietzelt M., Al Scharaa O., Tegtbur U., Haux R., Marschollek M., "Decision support for teletraining of COPD patients," *Pervasive Computing Technologies for Healthcare, 2009. Pervasive Health 2009. 3rd International Conf.,* vol., no., pp.1-6, 1-3 April 2009.

[14] Aroul, A.L.P., Bhatia, D., Estevez, L., "Energy-efficient ambulatory activity monitoring for disease management," *Medical Devices and Biosensors, 2008. ISSS-MDBS 2008. 5th International Summer School and Symp.,* vol., no., pp.201,204, 1-3 June 2008.

[15] Aroul A. L., Manohar, A., Bhatia D., Estevez L., "Power Efficient Multi-band Contextual Activity Monitoring for Assistive Environments," *Proceedings of the 1st International Conference on Pervasive Technologies Related to Assistive Environments. ACM International Conference Proceeding Series,* Vol. 282, p. 19, July 2008.

[16] Walker W., Polk T., Hande A., Bhatia D., "Remote Blood Pressure Monitoring Using a Wireless Sensor Network," *IEEE Sixth Annual Emerging Information Technology Conf.,* 2006.

[17] Walker W., Aroul A. L., & Bhatia D., "Mobile Health Monitoring Systems," *Engineering in Medicine and Biology Society, EMBC*, pp. 5199-5202, 2009.

[18] Mitchener J., "What we'll wear - [comms futures]," *Engineering & Technology*, vol.3, no.18, pp.74, October 25 2008.

[19] *Substrate: Background*, Cornell Centre for Materials Research: http://people.ccmr.cornell.edu/~cober/MSE5420/page2//files/iNEMISubstrateFlex0808.pdf

[20] S. Merilampi, T. Björninen, L. Ukkonen, P. Ruuskanen, L. Sydänheimo, "Printed Passive UHF RFID Tags as Wearable Strain Sensors," *3rd International Symposium on Applied Sciences in Biomedical and Communication Technologies (ISABEL)*, Rome, 2010

[21] Vallozzi L., Rogier H., and Hertleer C., "Dual polarized textile patch antenna for integration into protective garments," IEEE Antennas and Wireless Propagation Letters, 7:440–443, 2008.

[22] Shaozhen Z., Langley R., "Dual-Band Wearable Textile Antenna on an EBG Substrate," *Antennas and Propagation, IEEE Transactions on*, vol.57, no.4, pp.926-935, April 2009.

[23] Matthews J.C.G., Pettitt G., "Development of flexible, wearable antennas," *European Conference on Antennas and Propagation (EuCAP) 2009*, pp.273–277, 23–27 March 2009.

[24] Maleszka T., Preisner M., and Kabacik P., "Meshed ground plane structures for textile antennas", *European Conference on Antennas and Propagation (EuCAP)*, pp. 713–717, March 2009.

[25] Jung S. R., Yong S. C., Jae H. L., Youndo T., Sangwook N., Tae J. K., "Embroidered Wearable Multiresonant Folded Dipole Antenna for FM Reception," *Antennas and Wireless Propagation Letters, IEEE* , vol.9, no., pp.803-806, 2010.

[26] Park S., Mackenzie K., Jayaraman S., "The wearable motherboard: A framework for personalized mobile information processing (PMIP)," in *Proc. Design Automat. Conf.*, pp. 170–174, Jun. 2002.

[27] Post E. R., Orth, M., Russo P. R., Gershenfeld N., "E-broidery: Design and fabrication of textile-based computing," *IBM Systems Journal* , vol.39, no.3.4, pp.840-860, 2000.

[28] Edmison J., Jones M., Nakad Z., Martin T., "Using piezoelectric materials for wearable electronic textile," *in Proc. Int. Symp. Wearable Comput.*, pp. 41–48, Oct. 2002.

[29] Cottet D., Grzyb J., Kirstein T., and Tröster G., "Electrical characterization of textile transmission lines," *IEEE Trans. Adv. Packag.*, vol. 26, no. 2, pp. 182–190, May 2003.

[30] Edward T.C, "Foundations of interconnect and Microstrip Design," pp.161, John Wiley & Sons, 2000.

[31] Ponchak G.E., Katehi L.P.B., Tentzeris E.M., "Finite Ground Coplanar (FGC) Waveguide: It's Characteristics and Advantages For Use In RF and Wireless Communication Circuits," *3rd International Wireless Communications Conference (WCC '98) Digest*, San Diego, CA, Nov. 1–3, pp. 75–83, 1998.

[32] *Probe Selection Guide*, Cascade Microtech: http://www.cmicro.com/files/Probe-Selection-Guide.pdf; referred July 13, 2013.

[33] Solid State Technology "Printed electronics sector takes hard look at the flexible future". Available at Online: http://www.electroiq.com/articles/sst/2013/03/printed-electronics-sector-takes-hard-look-at-the-flexible-futur.html.

[34] Mäntysalo, M., Kaija, K., Koskinen, S., Nittynen J., "Inkjeted 3D Interconnections for Electronic Applications," *IMAPS workshop on printed devices and applications 2009*, Orlando, Florida USA, February 23-25,.

[35] Mäntysalo M., Mansikkamä P., "Inkjet-deposited interconnections for electronic packaging," *23rd International Conference on Digital Printing Technologies, Anchorage*, Alaska, USA, pp.813-817, Sept. 16-21, 2007.

[36] Enderling S., Brown C.L. III, Smith S., Dicks M.H., Stevenson J., Mitkova M., Kozicki M.N., Walton A.J., "Sheet resistance measurement of non-standard cleanroom materials using suspended Greek cross test structures," *Semiconductor Manufacturing, IEEE Transactions on*, vol.19, no.1, pp.2-9, Feb. 2006.

[37] Carver G.P., Matties R.L., Buehler M. G., "Design Considerations for the Cross-Bridge Sheet Resistor," *NBSIR 82-2548, National Bureau of Standards*, Washington, DC, 1982.

[38] Versnel W., "Analysis of the Greek cross, a Van der Pauw structure with finite contacts," *Solid State Electron*., vol.22, no.11, pp. 911-914, 1979.

[39] Carchon G., Nauwelaers B., "Accurate transmission line characterization on high and low-resistivity substrate," *IEEE Proceeding – Microwaves, Antennas and Propagation*, Vol.148, No.5, pp. 285-290, Oct. 2001.

[40] Mangan, A.M., Voinigescu, S. P., Yang, M. –T., Tazlauanu, M., "De-embedding transmission line measurements for accurate modeling of IC designs," *IEEE Trans. Electron Devices*, Vol. 53, No. 2, pp. 235-241, 2006.

[41] Sillanpää, H., Lilja, j, Mäkinen, R., Östman, K., Palukuru, V., Virtanen, J., Pynttäri, V., Kanerva, T, Hagberg, J., Lepistö, T, Jantunen, H., Mansikkamäki, p., "Application of wide-band material parameter extraction techniques to printable electronics characterization," *Proc. 59th Electronic Components and Technology Conf.*, San Diego, CA, pp. 1324-1348, May 2009.

[42] Sillanpää, H., Rasku, A., Mäkinen, R., "A multiline material parameter extraction method," *Proc. Mediterranean Microwave Symp*., Gyzelyurt, Cyprus, pp. 314-317, Aug. 2010.

[43] Rasku, A., Sillanpää, H., Hiltunen, I., Mäkinen, R., "Multiline material parameter extraction method performance analysis," *Proc. Asia-Pacific Microwave Conf., Yokohama*, Japan, pp. 1905-1908, Dec. 2010.

[44] Marks, R., B., " A multiline method of network analyser calibration,"*IEEE Trans*. *Microwave Theory Tech.*, Vol. 39, No.7, pp. 1205-1215, 1991.

[45] Pozar D. M., "Microwave Engineering", *3rd Edition. John Wiley & Sons, Inc.*, New York, p.49, 2007.

[46] Lilja, J., Sillanpää, H., Mäkinen, R., Palukuru, V., Östman, K., Hagberg, J., Kaneva, T., Jantunen, H., Lepistö, T., Mansikkamäki, P., "Wide-band characterization of printable electronics materials: the effect of conductor loss and internal inductance on relative permittivity," *3rd European conference on Antennas and Propagation, 2009*, Berlin, Germany, pp.3869-3873, March 23-27, 2009.

[47] Pozar D. M., "Microwave Engineering," *3rd Edition. John Wiley & Sons, Inc.*, New York, p.384, 2007.

[48] Davidson A., Strid E., Jones K., "Achieving greater on-wafer S-parameter accuracy with the LRM calibration technique," *ARFTG Conference Digest-Winter, 34th*, vol.16, no., pp.61-66, Nov. 30 1989-Dec. 1 1989.